Updated Reference Discrete Fracture Network Model at Utah FORGE

Aleta Finnila[1] and Clay Jones[2]

[1]WSP USA, Redmond, Washington, USA

[2]EGI at University of Utah, Salt Lake City, Utah, USA

aleta.finnila@wsp.com

Keywords: Utah FORGE, Enhanced Geothermal Systems (EGS), Discrete Fracture Network (DFN), k-means clustering, geologic model, fracture model.

ABSTRACT

The Reference Discrete Fracture Network (DFN) model for the Frontier Observatory for Research in Geothermal Energy (FORGE) site near Milford, Utah, is used to characterize both the natural fractures present in the reservoir and induced fractures created during hydraulic stimulation. The reservoir rock consists of crystalline granitic and metamorphic rock at around 8000 ft below the ground surface. The model can be used by researchers simulating processes such as well hydraulic stimulation, local stress evolution, flow pathway analysis, circulation tests, and thermal breakthrough. Previous versions of the Reference DFN were released in 2019 and 2021 with a minor update in 2023 to include fracture planes fit to the seismic point cloud generated from the stimulation of well 16A(78)-32. The 2019 DFN version was based on data from the vertical pilot well 58-32 while the 2021 revision included data sets from vertical well 56-32 and the highly deviated well 16(78)-32. New wells in the deep geothermal reservoir rock have been drilled since the last major revision in 2021: a vertical well, 78B-32, and a second highly deviated well, 16B(78)-32, having a lateral section parallel to and 330 ft above the lateral section of well 16A(78)-32. Data sets collected from these five wells have been analyzed to further constrain fracture orientations and intensity. The current interpretation of lithologic boundaries and significant fracture zones presented in this paper relies on the application of k-means cluster analysis to wireline log data and comparison of these results with available core samples.

1. INTRODUCTION

The Utah Frontier Observatory for Research in Geothermal Energy (FORGE) is a multi-year initiative funded by the US Department of Energy for testing targeted EGS research and development. The site is located inside the southeast margin of the Great Basin near the town of Milford, Utah, with hot granitic and metamorphic basement rocks at depths ranging from 2,550 to 9,500 ft (Figure 1). Three vertical wells and two highly deviated wells have been drilled in the targeted reservoir region. A Reference Discrete Fracture Network (DFN) model is used to characterize both the natural fractures present and the induced fractures created during hydraulic stimulation. The model is used by researchers simulating processes such as well hydraulic stimulation, local stress evolution, flow pathway analysis, circulation tests, and thermal breakthrough. Previous versions of the Reference DFN were released in 2019 and 2021 with a minor update in 2023 to include fracture planes fit to the seismic point cloud generated from the stimulation of well 16A(78)-32.

The initial DFN developed for FORGE was described in 2019 and was based on the data available at the time, primarily data from the vertical pilot well, 58-32, and outcrop data in the nearby mountain range (Finnila et al., 2019). Well 58-32 reached 7,536 ft in true vertical depth (TVD) measured from the ground surface with a measured depth along the borehole of 7,547 ft below ground surface (MDBGS). Three different fracture sets were characterized based on the Formation Micro Scanner (FMI) log interpretation of fracture orientations with the most prominent being a subvertical E-W striking set. The two other sets included one striking N-S and moderately dipping to the West, and a more steeply inclined NE-SW striking set dipping to the SE. Two regions of differing fracture intensity were observed, an 880 ft thick higher intensity zone at the top of the granitic basement rock and a lower intensity zone at deeper levels. The boundary between the higher intensity zone and the lower intensity zone corresponded with a compositional transition from Monzodiorite to Monzonite lithology based on analysis of drill cuttings collected at 100-foot intervals and a change from higher porosity to lower porosity as measured in the neutron porosity log. The deeper, lower intensity zone was interpreted to be characteristic of the rock at reservoir depths and therefore used for the DFN. Fracture sizes were parameterized based on mapped trace length data in nearby rock outcrops using both log normal and power law distributions with the log normal parameterization ultimately used for the DFN. Fracture shapes were considered be roughly circular based on their location in non-layered intrusive bodies and modeled for convenience using hexagonal shapes. Most of the fractures in the DFN were generated stochastically, however, the stochastic fractures that intersected well 58-32 were replaced with a discrete set of fractures as identified from the well log where their locations and orientations were know.

A model revision in 2021 incorporated additional data from two additional wells in the reservoir: another deeper vertical well, 56-32, and the highly deviated well, 16A(78)-32 (Finnila et al., 2021; Fu et al., 2024). Well 56-32 reached 9,107 ft TVD (9,115 ft MDBGS) while well 16A(78)-32 has a maximum depth of 8,565 ft TVD (10,937 ft MDBGS). Based on the Thru Bit FMI log of well 16A(78)-32, a fourth fracture set was added to the DFN (vertical SSW striking) and the mean set pole orientations and concentration parameters of the Fisher distributions of the previous three sets from the 2021 model were adjusted. Fracture orientations in well 56-32 were very similar to those found in well 58-32 while the fractures interpreted from the 16A(78)-32 FMI log were primarily in the new, fourth set

(which was not found in either of the vertical wells). As the quality of the FMI log was not as high in well 16A(78)-32, this difference was tentatively ascribed to bias in the well 16A(78)-32 log interpretation. Average fracture intensity for the DFN was estimated in the deep reservoir by integrating the FMI data coming from all three wells, with more weight given to the vertical wells where there was greater confidence in the fracture identification. Well 16A(32)-78 had approximately half the fracture intensity seen in the two vertical wells. Fracture sizes were parameterized using a truncated power law distribution having a power law exponent of 3.2 and a minimum fracture radius of 0.63 m (Finnila, 2021). A deterministic set for fractures intersecting well 16A(78)-32 was included based on those features identified in the FMI log interpretation. Fracture sizes of this deterministic set were generated using the same truncated power law distribution as the stochastic set, but only those larger than the minimum DFN size cutoff of 10 m radius were kept in the model.
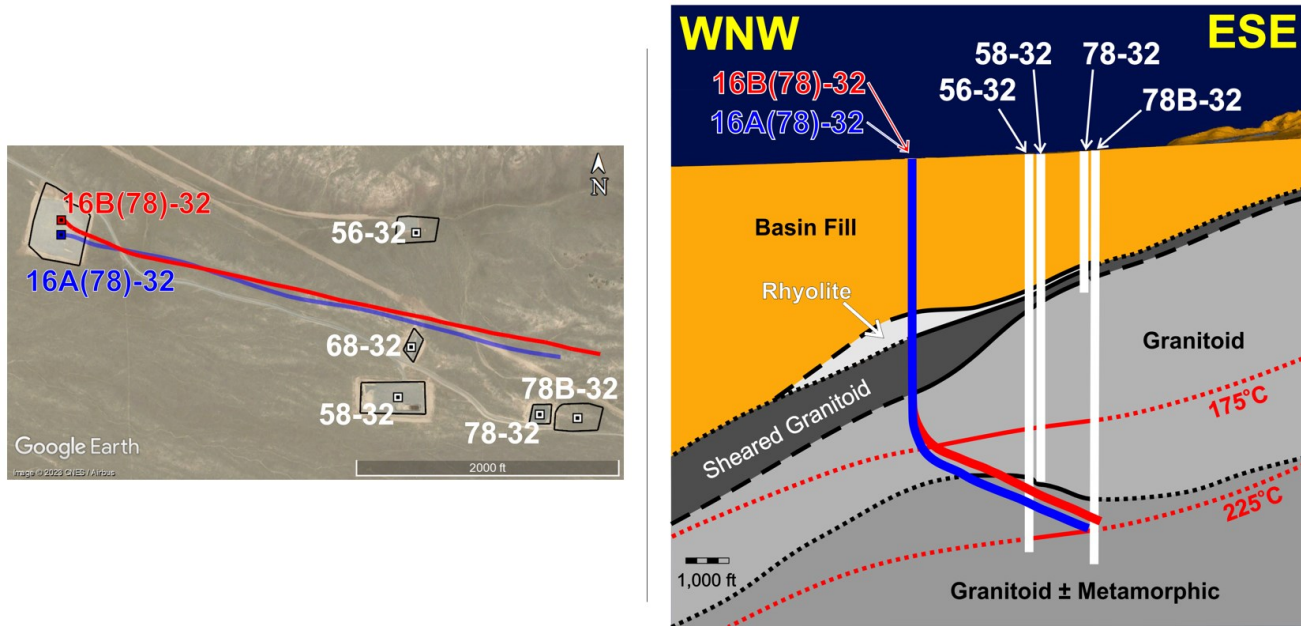

Figure 1: Satellite map and cross-section of the Utah FORGE EGS site. The cross section is parallel to the trajectory of well 16A(78)-32 showing: deep wells (>1,000 ft) drilled at the site to date; lithologies encountered in the wellbores; inferred temperature contours in the subsurface.

Following the stimulation of well 16A(78)-32 in 2022, a small DFN was created to capture planar features identified from the Microearthquake catalog (Finnila et al., 2023). These planar features were interpreted to be large fractures or collections of smaller fractures sharing common orientations and locations. Fifteen hexagonal fractures are included in this model: eleven were fit from the microseismic data and four were added based on previous FORGE DFN characterization work to provide connectivity between the fractures and the injection intervals. This small DFN model has been used both by itself and in combination with the larger 2021 Reference DFN by FORGE modeling teams (Radakovic-Guzina et al, 2024). It provided an alternative fracture network having fewer discrete features and attempted to capture the most significant flow pathways created by the stimulation of 16A(78)-32. Uncertainty in locations of the events recorded during stimulation of Stages 1 and 2 (and consequently in the geometry of the inferred fractures) is much greater than that for Stage 3 because during Stages 1 and 2 fewer, more distant geophones were used to record microseismicity.

Data sets from two more deep wells are now available and are included in this new revision to the FORGE Reference DFN as described in this paper. Well 78B-32 is vertical with a maximum depth of 9,468 ft TVD (9,471 ft MDBGS) and well 16B(78)-32 is highly deviated like 16A(78)-32 with a maximum depth of 8,352 ft TVD (10,915 ft MDBGS). In addition to providing simple updates to the DFN fracture set orientations and intensities, the hope for this new revision is to also address the following outstanding questions:

- Do we have sufficient data now to subdivide the Reference DFN into different regions having distinct fracture set populations based on fracture orientations or intensity? An example might be the distinction between the granitoid lithology and the mixed granitoid and metamorphic lithologies shown in Figure 1.

- Can we identify any significant faults or fracture zones that can be added to the DFN as discrete features?

- Can we provide a rationale for selecting which identified fractures from the well logs to include in the discrete fracture set? This might involve ranking the identified fractures by interpreted hydraulic significance.

- Can we explain why the interpreted fracture orientations and intensities were so different in well 16A(78)-32 vs the two vertical wells 58-32 and 56-32 used in the 2021 DFN?

- Does the DFN show connectivity that is consistent with well testing data?

While the current work does not completely answer these questions, there is some progress which justifies a revision to the Reference DFN model. The following paper sections describe the progress to date and remaining issues will be highlighted in the Discussion section at the end.

2. SUBDIVIDING THE DFN INTO REGIONS

In order to determine if subdividing the DFN region is justified, we thought it would be helpful to examine fracture orientations and intensities in different regions of the reservoir to see if they differ by location. Previous work on core samples and drilling chips shows that the lithology rapidly changes in both composition and texture over a wide range of both plutonic and metamorphic lithologies (Jones et al., 2021). Using k-means clustering techniques on the various log data sets available provides one method of grouping well intervals by rock type or structure. This method was previously used for well 56-32 to divide the ThruBit Dipole acoustic log data for the interval between 3423 ft MDBGS and 9005 ft MDBGS into five categories: altered rock; Qtz-poor, plutonic rock; Qtz-rich, high-K plutonic rock, mixed plutonic rock and gneiss; and highly fractured zones (Finnila and Jones, 2022). A similar workflow was followed for the current work by using acoustic log data from all five wells in the clustering analysis. In the following subsections we describe the workflow, show the results for various choices of the number of clusters, and compare the results with available core.

2.1 K-Cluster Methodology

Ideally, for the cluster analysis we would like to have data from the same tool for each well. This was not possible for the five deep wells at FORGE, however, the acoustic log data seemed very similar across the well data sets so that was the final choice after experimenting with various log combinations. The data sources are listed in Table 1 along with the parameters selected for inclusion in the cluster analysis.

Table 1. Acoustic log data sources used for k-cluster analysis.

Well	Log File	Parameters Used in K-Clustering	Reference
58-32	UniversityOfUtah_MU-ESW1_DSI_PnS-Aniso_FirstPass.las	MD[ft]; DTSM_FAST[µs/ft]; GR_EDTC[gAPI]; PR[-]; SPHI[ft3/ft3]; TNPH[ft3/ft3]	EGI, 2018
56-32	University_of_Utah_Forge_56_32_ThrubitDipole_Aniso_analysis_result_3452-9050ft_LAS.las	MD[ft]; DTSH_FAST[µs/ft]; GR_TMG[gAPI]; PR[-]; SPHI[ft3/ft3]; TNPH[ft3/ft3]	EGI, 2021a
16A(78)-32	University_of_Utah_Forge_16A_78-32_ThrubitDipole_PNS_result_5000-10940ft.las	TDEP[ft]; DTSH_PNS_final[µs/ft]; GR_TMG[gAPI]; PR[-]; SPHI[ft3/ft3]; TNPH[ft3/ft3]	EGI, 2021b
78B-32	UOU_FORGE-78B-32_R1B_5.75in_QSLT_SONIC_PnS_7495-9540ft_LAS.las	TDEP[ft]; DTSH_FINAL[µs/ft]; GR_STGC[gAPI]; PR[-]; SPHI[ft3/ft3]; TNPH[ft3/ft3]	EGI, 2021c
16B(78)-32	University_of_Utah_Utah_Forge_Forge_16B_78-32_9.5in_TBDS_PNS_ANISO_4835ft-10872ft_LAS.las	MD[ft]; DTSH_FAST[µs/ft]; GR_TMG[gAPI]; PR_FAST[-]; SPHI[ft3/ft3]; TNPH[ft3/ft3]	EGI, 2023

After loading the acoustic log data for each well, depth values missing any of the selected parameters was discarded as missing values are not allowed for the clustering algorithm. This left 53,831 rows of data indexed by well and depth (Figure 2).

	MD[ft]	DTSH[us/ft]	GR_TMG[gAPI]	PR[-]	SPHI[ft3/ft3]	TNPH[ft3/ft3]
count	54046	53981	54046	53831	53858	54046
mean	7049.39	98.38	141.02	0.28	0.05	0.05
std	2038.95	13.17	64.53	0.04	0.04	0.04
min	2155.00	66.53	6.60	0.04	0.00	-0.02
25%	5549.13	92.71	89.56	0.25	0.03	0.02
50%	7238.00	95.39	136.99	0.28	0.04	0.04
75%	8638.69	98.95	176.11	0.30	0.05	0.06
max	10940.00	206.84	738.70	0.40	0.37	0.58

Figure 2. Parameter value distributions with high and low count values of non-missing data color coded high (red) to low (blue).

Quick checks of the data distributions are examined using histograms (Figure 3) and a correlation matrix is produced to check for significant depth dependency or linear relationships between parameters (**Error! Reference source not found.**).
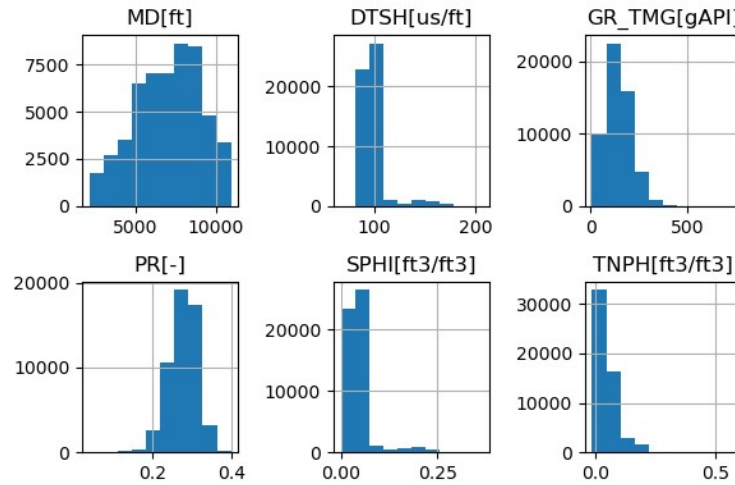

Figure 3. Histograms of acoustic data parameter values selected for cluster analysis in the five deep FORGE wells.
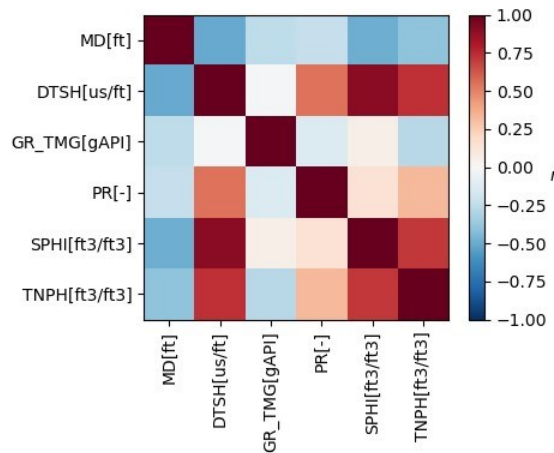

Figure 4. Correlation matrix for selected acoustic parameters values in the five deep FORGE wells.

It is also instructive to show the property values mapped onto the wells to get a preview of what patterns may be present in the data. Figure 5 shows an example of this using the Gamma Ray property in the reservoir. We use the WSP FracMan software suite (WSP UK, 2023) to visualize the data and perform various analyses for the DFN parameterization. Figure 6 shows a close up of the property values in the vertical sections of wells 16A(78)-32 and 16B(78)-32. If the tools and data processing methods were the same for both wells, and the lithology was consistent between the two, we would expect to see very similar values between these two wells as they are located less than 100 feet from each other. The systematic difference visible in the thermal neutron porosity (TNPH) property is unfortunate and may be due to having potentially used different reference lithologies in the ratio method, however, similar results were obtained when this property was removed from the analysis so keeping it in the clustering analysis was considered to be reasonable.
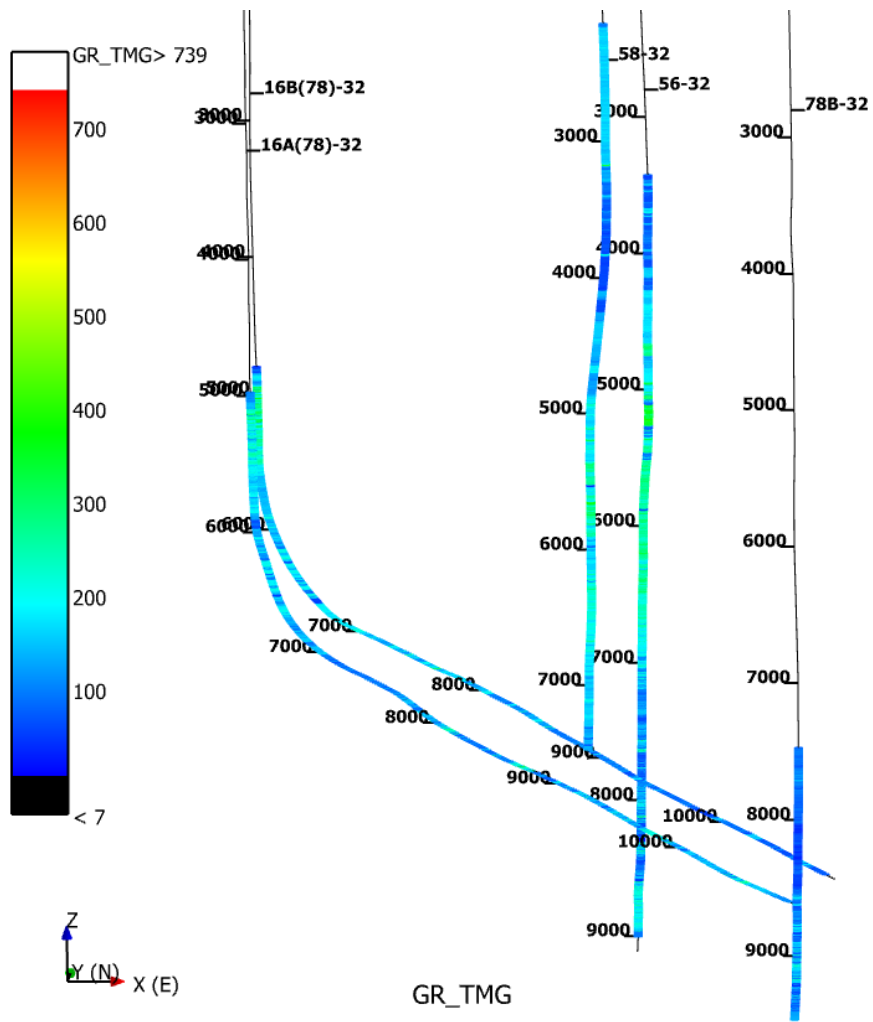
Figure 5. Gamma Ray property mapped onto the five deep wells with depth from ground surface [ft] indicated for each well.
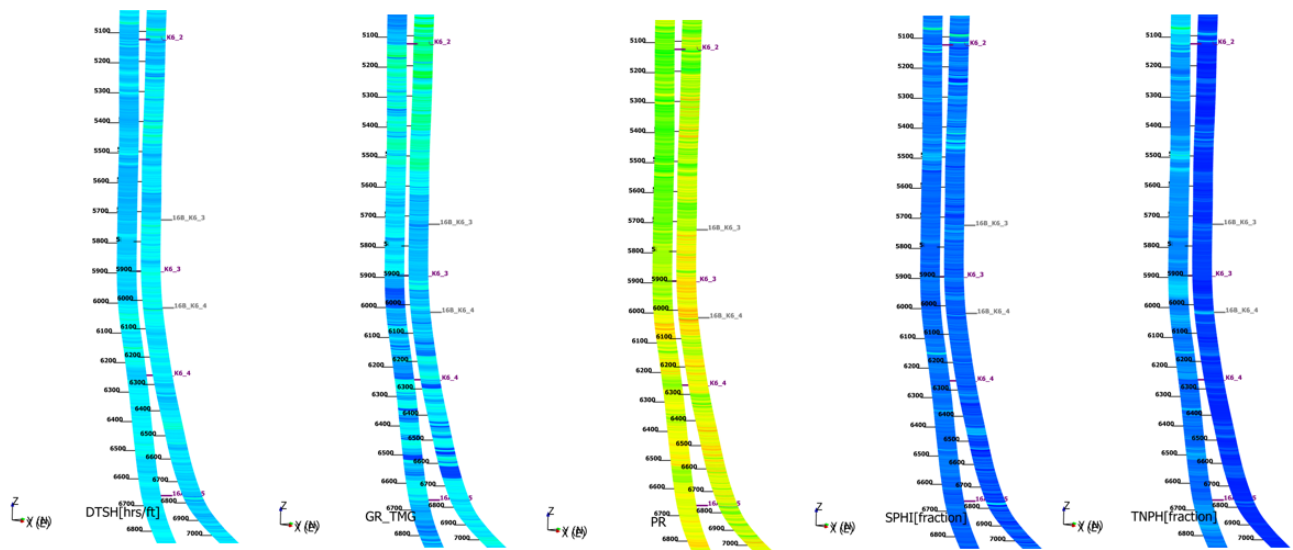

Figure 6. Acoustic property comparison at the vertical sections of wells 16A(78)-32 and 16B(78)-32.

Once the set of acoustic properties was selected, the values were normalized, and a Principal Component Analysis was performed which reduced the problem dimensionality from 5 to 4. The transformed data was then used in the cluster analysis using a range of k values (this is the number of groups to use when dividing the data). Since we do not know how many different physically distinct rock types we are looking for, it is standard to create an elbow plot of inertia vs the number of clusters used in the k-means clustering to look for obvious "kinks" that might reasonable choices for the number of clusters present in the data. Inertia is the sum of squared distance of samples to their closest cluster center. The inertia will drop to 0 as the number of clusters approaches the number of samples. The most significant kinks occur at k-values of 2, 3, and 4, but they are not very pronounced.
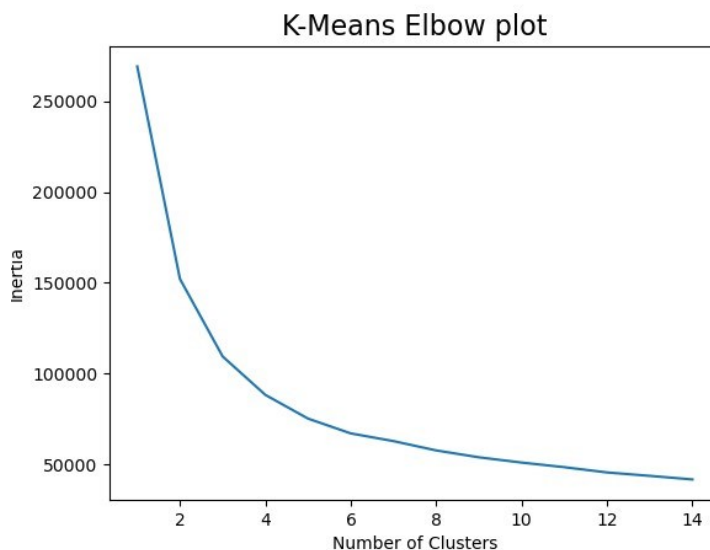

Figure 7. Elbow plot used to help determine the number of clusters naturally present in a data set.

Since the elbow plot does not strongly indicate a particular choice in the number of clusters, the k-clustering was performed for a range of values between 2 and 10.

2.2 K-Cluster Results

Note that all depths shown in the figures included in this section are referenced from the well Kelly-Bushing (KB) as this was the point of reference with regards to well logging and core collection. The KB height for 58-32 was 21.5 ft, for 56-32 it was 30.4 ft, for 78B-32 it was 29.5 ft, for 16A(78)-32 it was 30 ft, and for 16B(78)-32 it was 32 ft. All data collected at the site can be accessed through the Geothermal Data Repository (GDR: https://gdr.openei.org/home). Units used in these reports are mix of imperial (i.e. all depths in feet), and metric to be consistent with the data collected at the site and that is available for download.

2.2.1 Two Cluster Results

When dividing the acoustic data into two groups, the alluvium in well 58-32 is immediately identifiable (see Figure 8 for an example showing the Shear Slowness as a function of depth for each well log). In Figure 8, the label 0 (blue) is interpreted to be bedrock and 1 (red) is interpreted to be alluvium. This is reassuring in the sense that the algorithm should be able to differentiate between unconsolidated fill and bedrock, but not immediately useful. There are traces of the "1" label in the bedrock depths shown in the logs for all of the wells except for 78B-32 where the Shear Slowness values are especially high. These may indicate rubble zones from faults or large fractures that could be added as discrete features to the Reference DFN. The black solid line indicates an interpreted significant boundary that may be of interest when subdividing the DFN into different regions. In this case where we only separate out the alluvium, it will not affect the DFN since the fracture model does not extend into the alluvium.
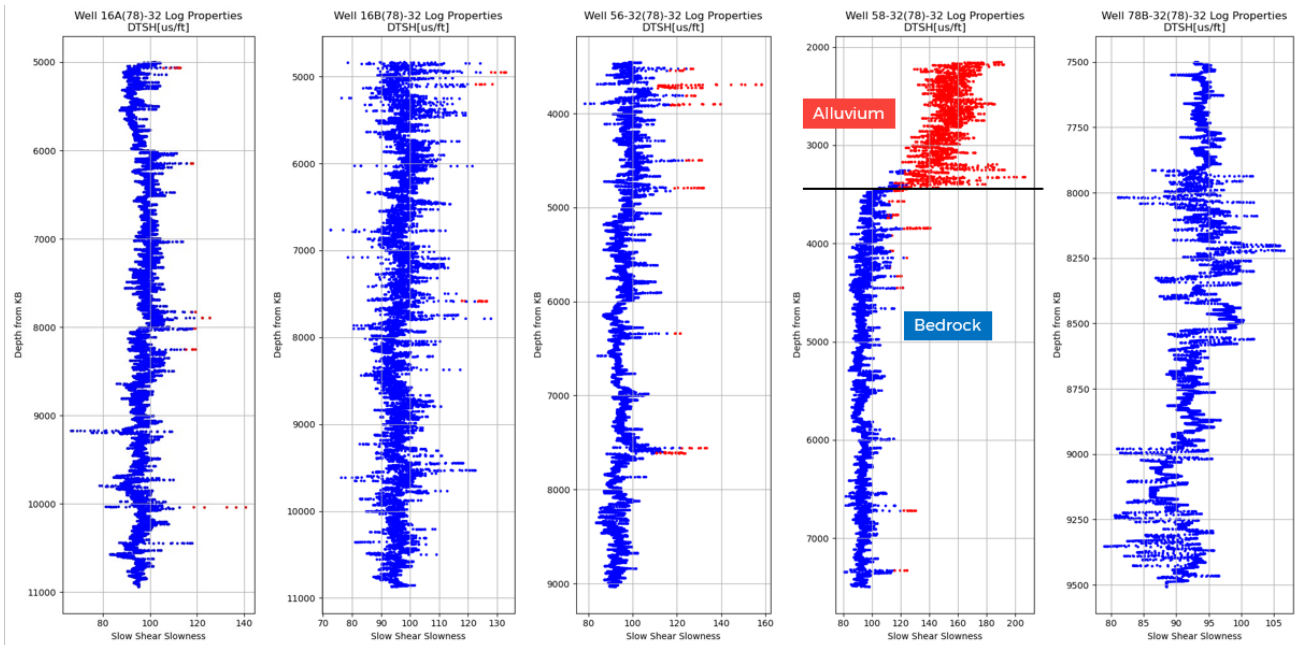
Figure 8. Shear slowness vs depth [ft] from KB by well with colors indicating labels from cluster analysis using k=2. The label 0 (blue) is interpreted to be bedrock and 1 (red) is interpreted to be alluvium.

2.2.2 Three Cluster Results

Once we increase the number of clusters to three, we start seeing divisions in the bedrock lithologies. Figure 9 shows gamma ray vs depth for the five wells with the colors indicating the cluster group: the label "0" (blue) is interpreted to be non-weathered or sheared bedrock; the label "1" (red) is interpreted to be alluvium; and the label "2" (grey) is interpreted to be weathered or sheared bedrock in well 58-32 while it seems likely to indicate generally lower gamma ray values in the other wells. The solid black lines may be showing the boundaries to the sheared granite near the bedrock surface.
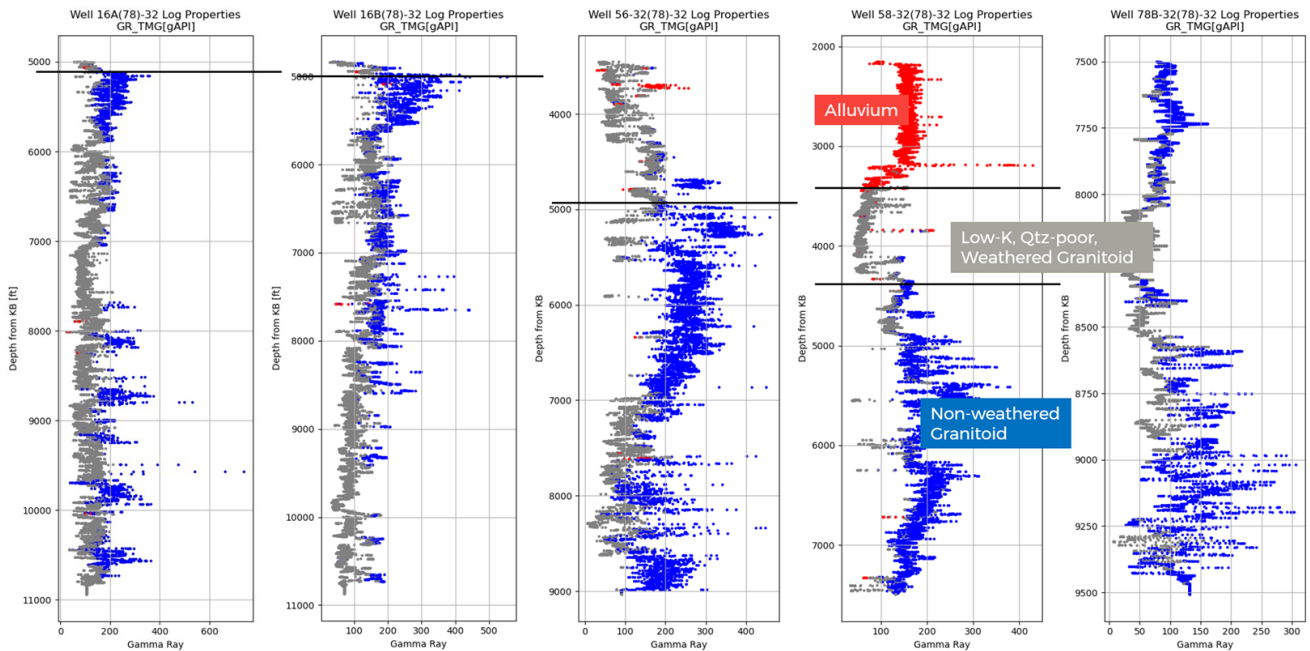

Figure 9. Gamma ray vs depth [ft] from KB by well with colors indicating labels from cluster analysis using k=3. The label "0" (blue) is interpreted to be non-weathered or sheared bedrock; the label "1" (red) is interpreted to be alluvium; and the label "2" (grey) is interpreted to be weathered or sheared bedrock.

2.2.3 Four Cluster Results

Moving on to using four clusters, there seem to be some correlations possibly apparent between the wells that may be useful for identifying distinct subregions to characterize the fractures. For example, in Figure 10, which shows the total porosity from sonic (SPHI) vs depth from KB, the deep zone colored grey in well 56-32 seems to match the grey interval in well 78B-32.
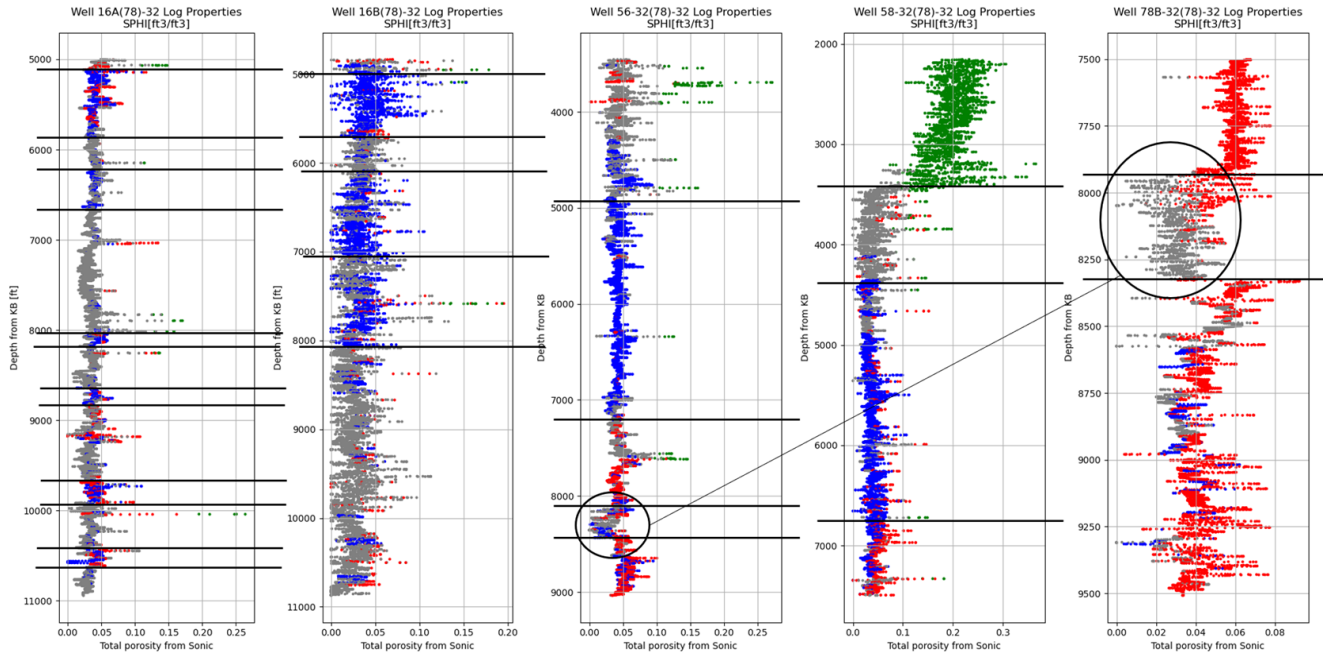

Figure 10. Total porosity from sonic vs depth [ft] from KB by well with colors indicating labels from cluster analysis using k=4. Black solid lines indicate potential significant rock type boundaries while the circled region may be correlated.

2.2.4 Five Cluster Results

With five clusters, we still seem to be finding more potential lithology changes, although the lack of correlation between wells 16A(78)-32 and 16B(78)-32 is disappointing given their close proximity. In general, the acoustic log values seem noisier in 16B(78)-32.
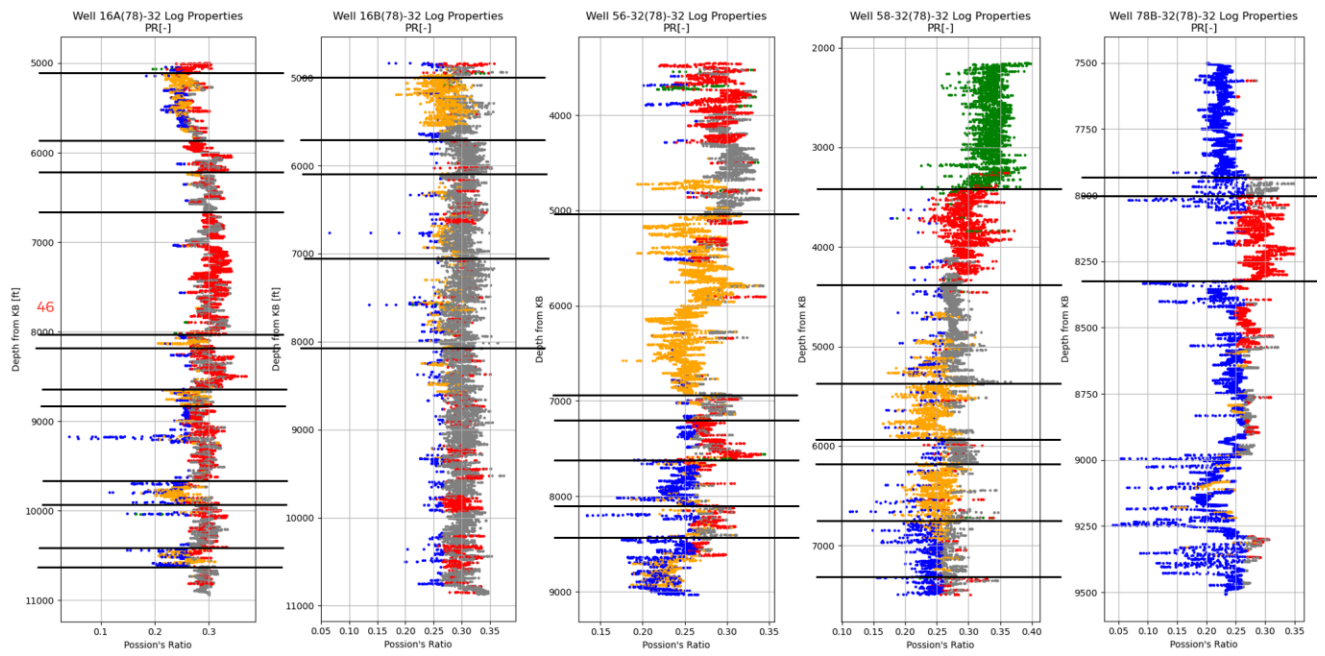

Figure 11. Poisson's ratio vs depth [ft] from KB by well with colors indicating labels from cluster analysis using k=5. Black solid lines indicate potential significant rock type boundaries.

2.2.5 Six Cluster Results

Six clusters seem to be giving enough detail to identify changing lithology, so we do not present results for higher numbers of groupings. For the DFN, we do not need to know all the minor lithology changes, just those that will affect the fracture model in a significant way. Figure 12 through Figure 16 show all five acoustic log properties that were used in the cluster analysis vs depth and colored by their cluster label. The black solid lines indicate the interval boundaries that are used to examine potential changes to fracture orientation or intensity.
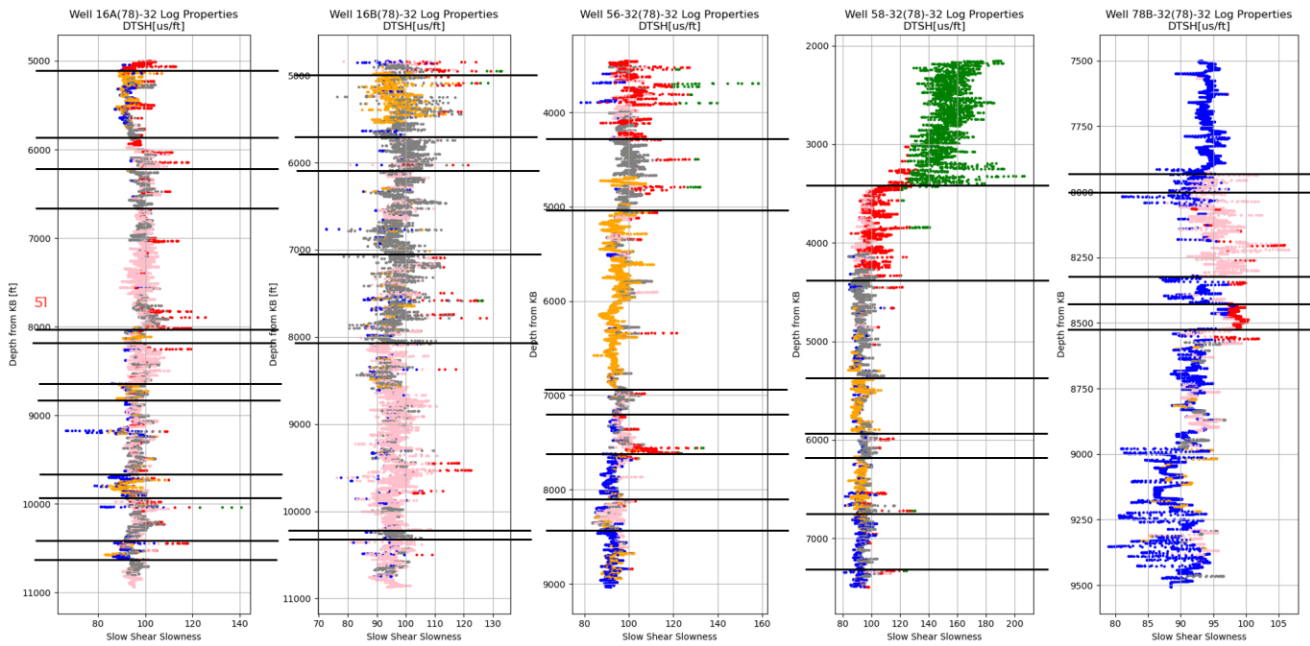

Figure 12. Shear slowness vs depth [ft] from KB by well with colors indicating labels from cluster analysis using k=6. Black solid lines indicate potential significant rock type boundaries.
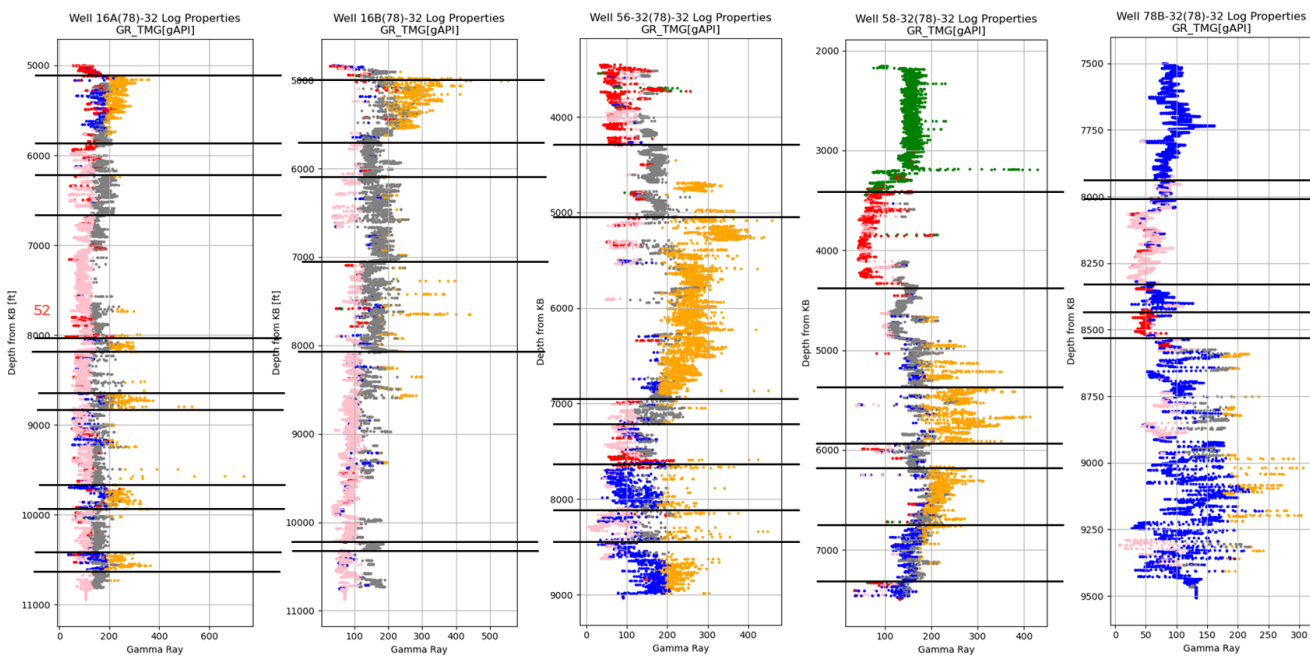

Figure 13. Gamma ray vs depth [ft] from KB by well with colors indicating labels from cluster analysis using k=6. Black solid lines indicate potential significant rock type boundaries.

9
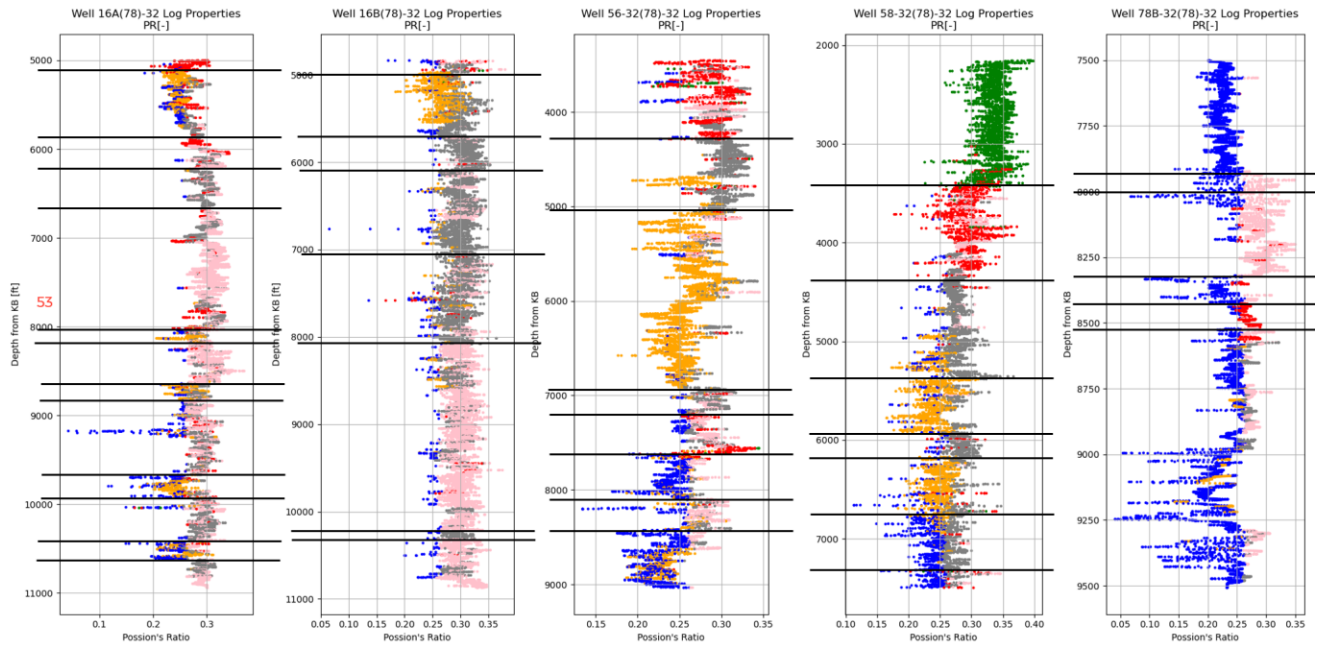
Figure 14. Poisson's ratio vs depth [ft] from KB by well with colors indicating labels from cluster analysis using k=6. Black solid lines indicate potential significant rock type boundaries.

Figure 15. Total porosity from sonic vs depth [ft] from KB by well with colors indicating labels from cluster analysis using k=6. Black solid lines indicate potential significant rock type boundaries.

Figure 16. Thermal neutron porosity vs depth [ft] from KB by well with colors indicating labels from cluster analysis using k=6. Black solid lines indicate potential significant rock type boundaries.
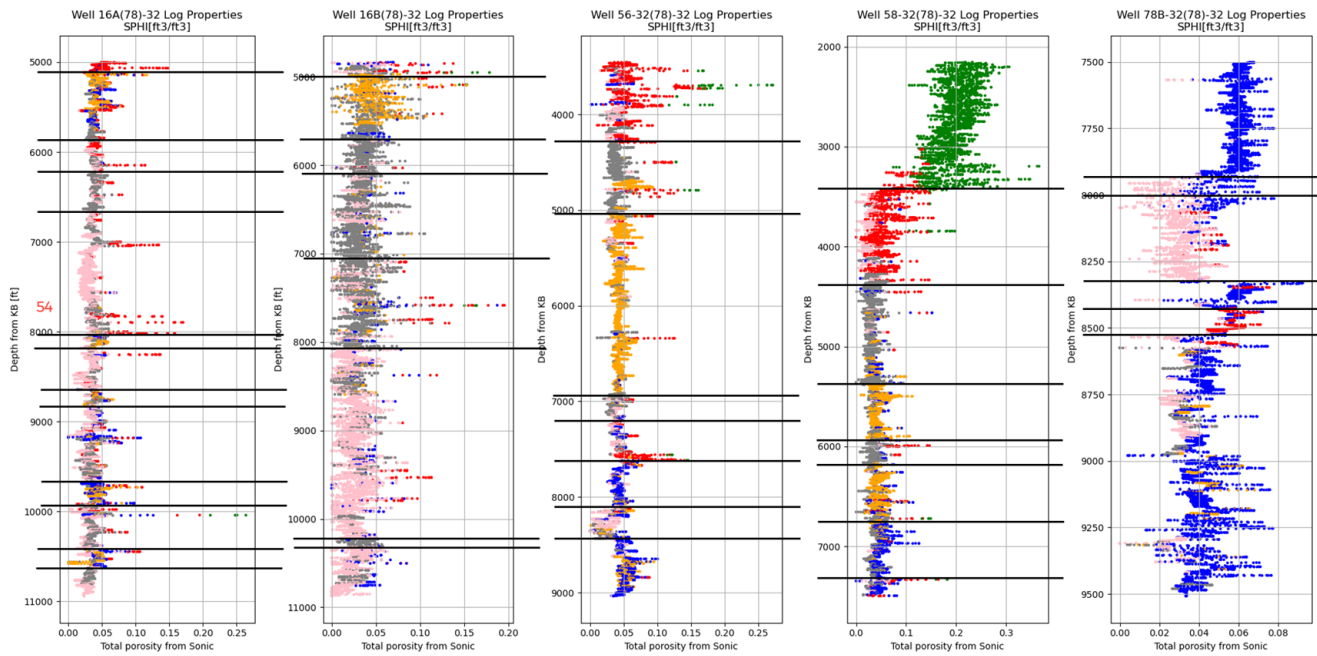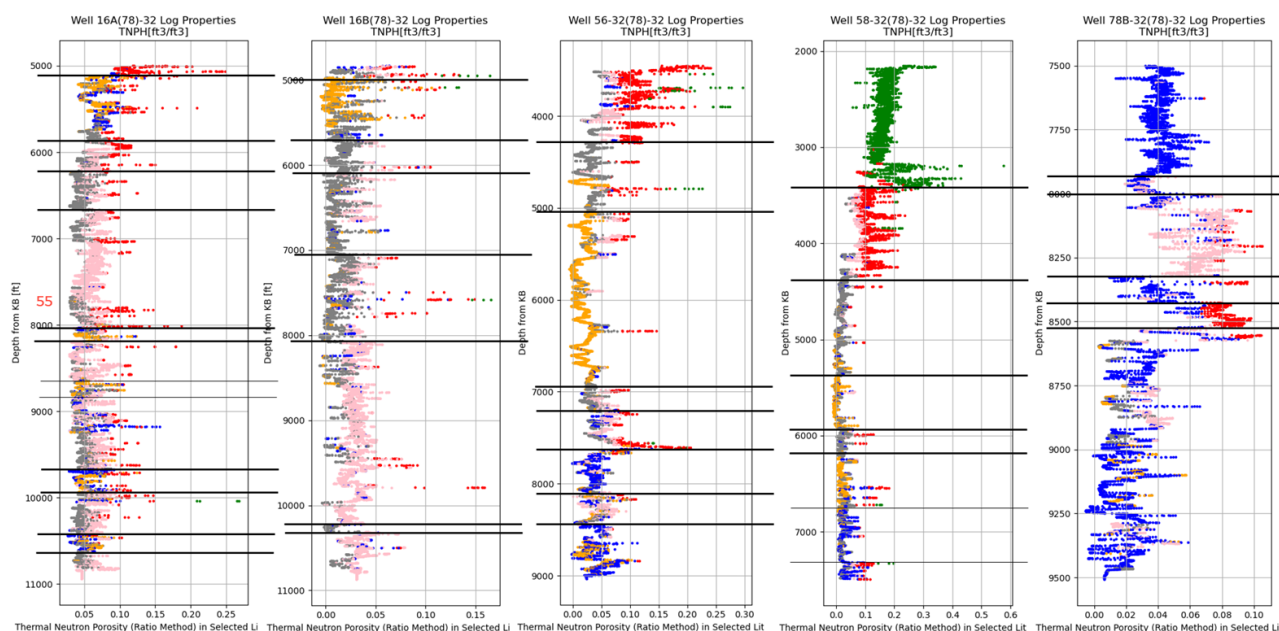
Figure 17 shows the mean values of the acoustic properties (and depth) for each cluster group. Each column in the table is colored from high value (red) to low value (blue). For example, the cluster label "0" occurs mostly at the deepest portions sampled by the wells, has the lowest values for shear slowness (DTSH) and Poisson's ratio (PR), somewhat low values for gamma ray (GR_TMG) and thermal neutron porosity (TNPH), and average values for total porosity from sonic (SPHI).

6_Lith_Category	MD[ft]	DTSH[us/ft]	GR_TMG[gAPI]	PR[-]	SPHI[ft3/ft3]	TNPH[ft3/ft3]
0 (blue)	8105	91.7	112.8	0.227	0.048	0.035
1 (red)	5477	102.9	89.6	0.286	0.061	0.110
2 (grey)	6836	96.8	163.7	0.291	0.035	0.027
3 (green)	2850	151.5	149.8	0.333	0.197	0.176
4 (orange)	6447	93.6	248.3	0.252	0.044	0.023
5 (pink)	8129	96.5	85.6	0.297	0.030	0.048

Figure 17. Mean values for acoustic properties by cluster label using k=6.

The rock type boundaries selected from the cluster results and shown as solid black lines in Figure 12 through Figure 16 are listed in Table 2. These are used to subset the identified fractures identified from resistivity logs in order to compare orientations and intensity.

Table 2. Well intervals from cluster analysis using k=6.

Well	Interval Name	Start Depth KB [ft]	End Depth KB [ft]	Interval Length [ft]
16A(78)-32	16A_K6_1	5001.5	5122.5	121.0
	16A_K6_2	5122.5	5894.0	771.5
	16A_K6_3	5894.0	6243.0	349.0
	16A_K6_4	6243.0	6661.5	418.5
	16A_K6_5	6661.5	8036.5	1375.0
	16A_K6_6	8036.5	8187.5	151.0
	16A_K6_7	8187.5	8654.0	466.5

11

	16A_K6_8	8654.0	8828.5	174.5
	16A_K6_9	8828.5	9671.0	842.5
	16A_K6_10	9671.0	9938.0	267.0
	16A_K6_11	9938.0	10432.5	494.5
	16A_K6_12	10432.5	10622.0	189.5
	16A_K6_13	10622.0	10940.0	318.0
16B(78)-32	16B_K6_1	4835.0	4951.0	116.0
	16B_K6_2	4951.0	5727.5	776.5
	16B_K6_3	5727.5	6026.5	299.0
	16B_K6_4	6026.5	7092.5	1066.0
	16B_K6_5	7092.5	8085.0	992.5
	16B_K6_6	8085.0	10227.5	2142.5
	16B_K6_7	10227.5	10317.0	89.5
	16B_K6_8	10317.0	10872.0	555.0
56-32	56-32_K6_1	3454.0	4295.5	841.5
	56-32_K6_2	4295.5	5063.0	767.5
	56-32_K6_3	5063.0	6915.5	1852.5
	56-32_K6_4	6915.5	7219.5	304.0
	56-32_K6_5	7219.5	7620.0	400.5
	56-32_K6_6	7620.0	8095.0	475.0
	56-32_K6_7	8095.0	8421.0	326.0
	56-32_K6_8	8421.0	9036.5	615.5
58-32	58-32_K6_1	2155	3409	1254.0
	58-32_K6_2	3409	4272.5	863.5
	58-32_K6_3	4272.5	5381	1108.5
	58-32_K6_4	5381	5923	542.0
	58-32_K6_5	5923	6169.5	246.5
	58-32_K6_6	6169.5	6721	551.5
	58-32_K6_7	6721	7330	609.0
	58-32_K6_8	7330	7497	167.0
78B-32	78B-32_K6_1	7501.3	7935.5	434.3
	78B-32_K6_2	7935.5	8000.0	64.5
	78B-32_K6_3	8000.0	8324.3	324.3
	78B-32_K6_4	8324.3	8344.8	20.5

78B-32_K6_5	8344.8	8519.3	174.5
78B-32_K6_6	8519.3	9507.8	988.5

2.3 Comparison of K-Cluster Results with Core

Since we have core samples from well 16B(78)-32 that were collected in portions of the well that we also have the acoustic log data, we can compare the clustering results with what we see in the core to see if our results are consistent. Figure 18 through Figure 22 show some examples of this comparison and the correspondence seems reasonable. Where the cluster labels change, there appears to be visible changes in core and when the cluster labels are constant, the core looks the same throughout.
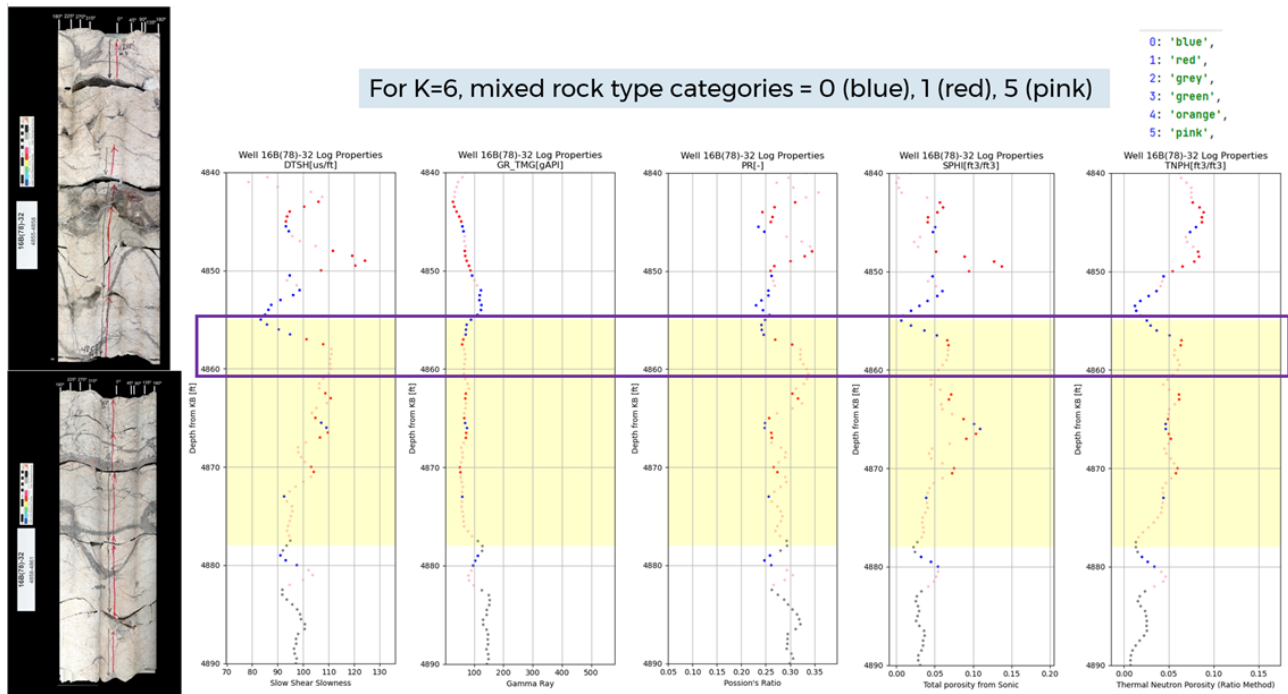

Figure 18. Comparing core from 16B(78)-32 at 4,855 ft KB to 10,4861 ft KB to cluster label using k=6. Shaded yellow region indicates where core is available.
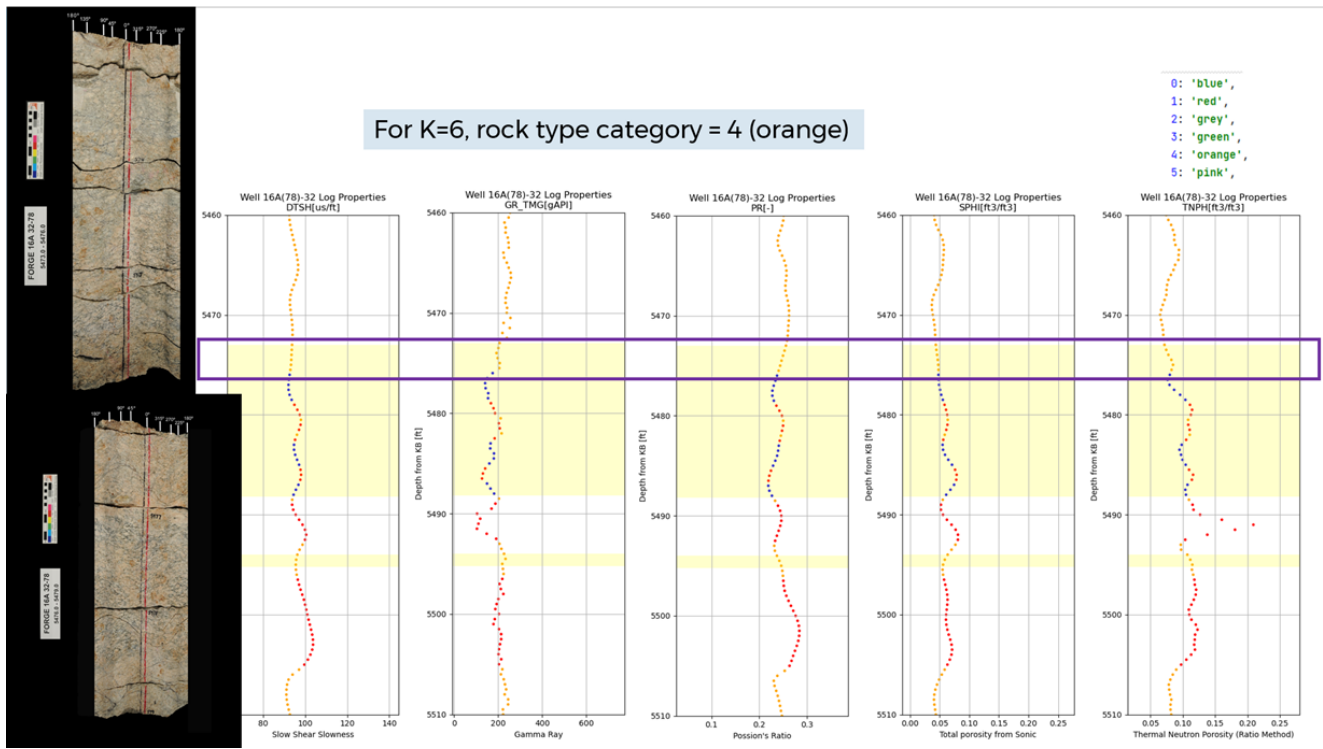
Figure 19. Comparing core from 16B(78)-32 at 5,473 ft KB to 5,479 ft KB to cluster label using k=6. Shaded yellow regions indicate where core is available.
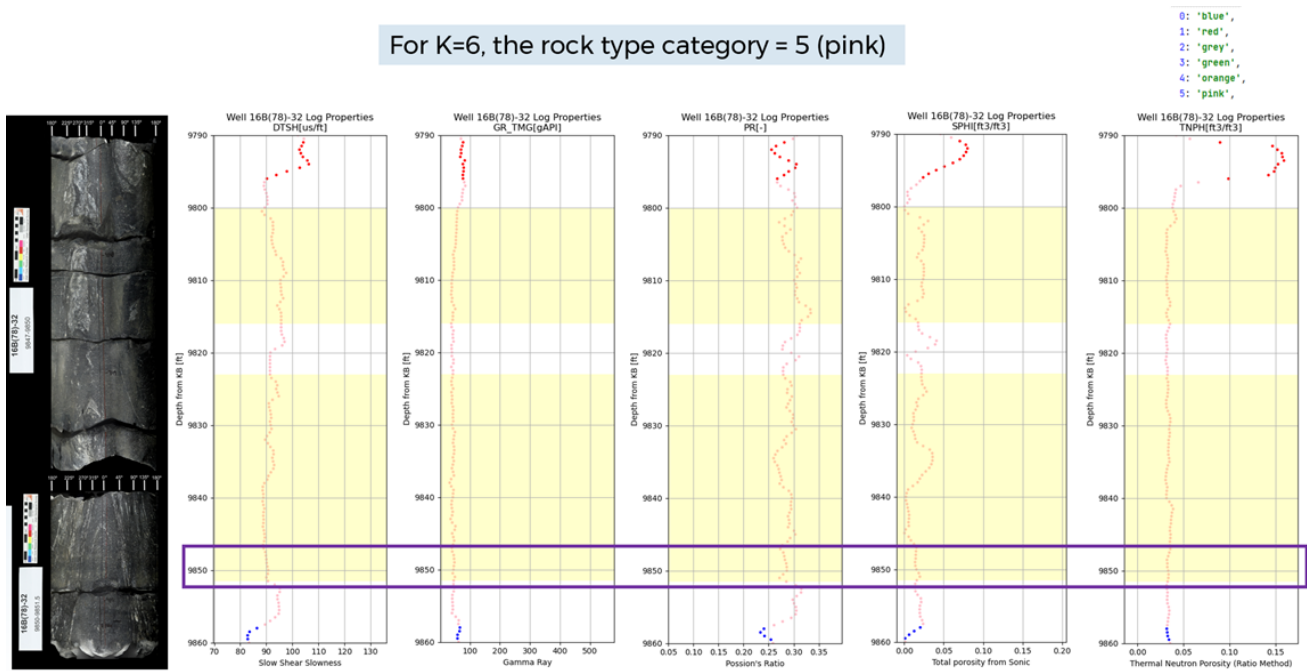

Figure 20. Comparing core from 16B(78)-32 at 9,847 ft KB to 9,851.5 ft KB to cluster label using k=6. Shaded yellow regions indicate where core is available.
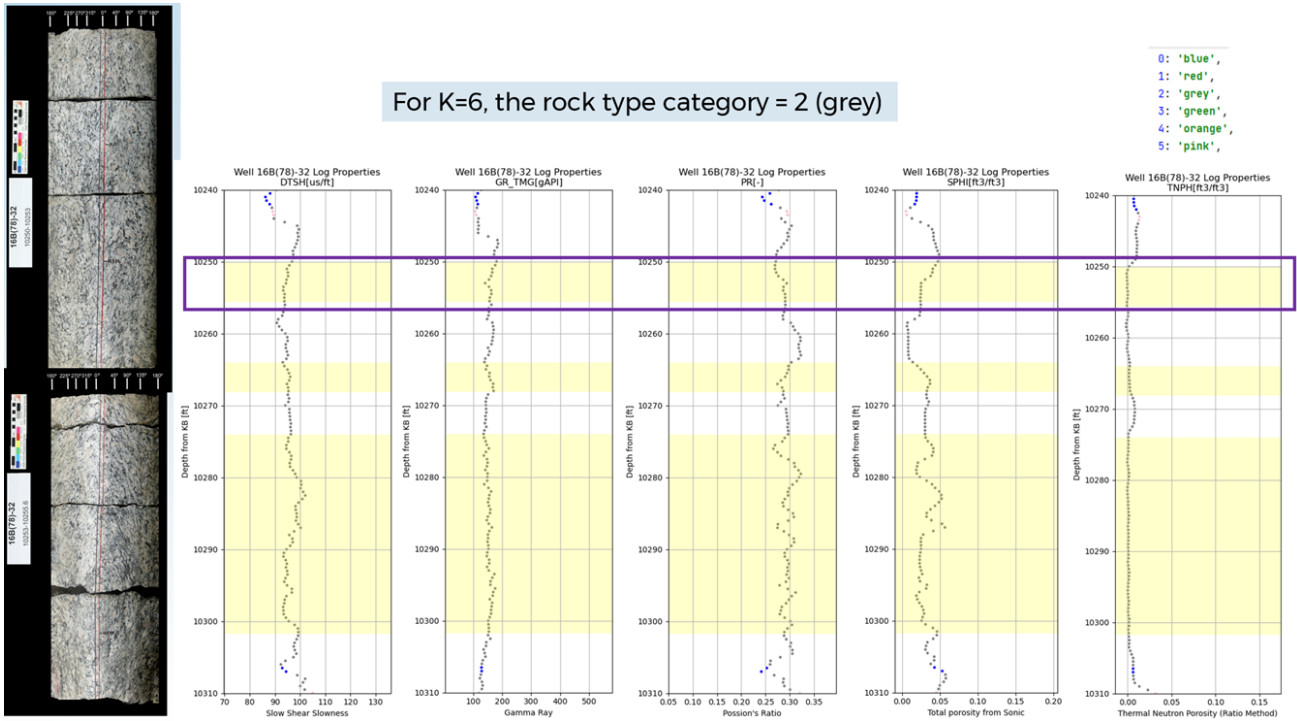
Figure 21. Comparing core from 16B(78)-32 at 10,250 ft KB to 10,255.6 ft KB to cluster label using k=6. Shaded yellow regions indicate where core is available.
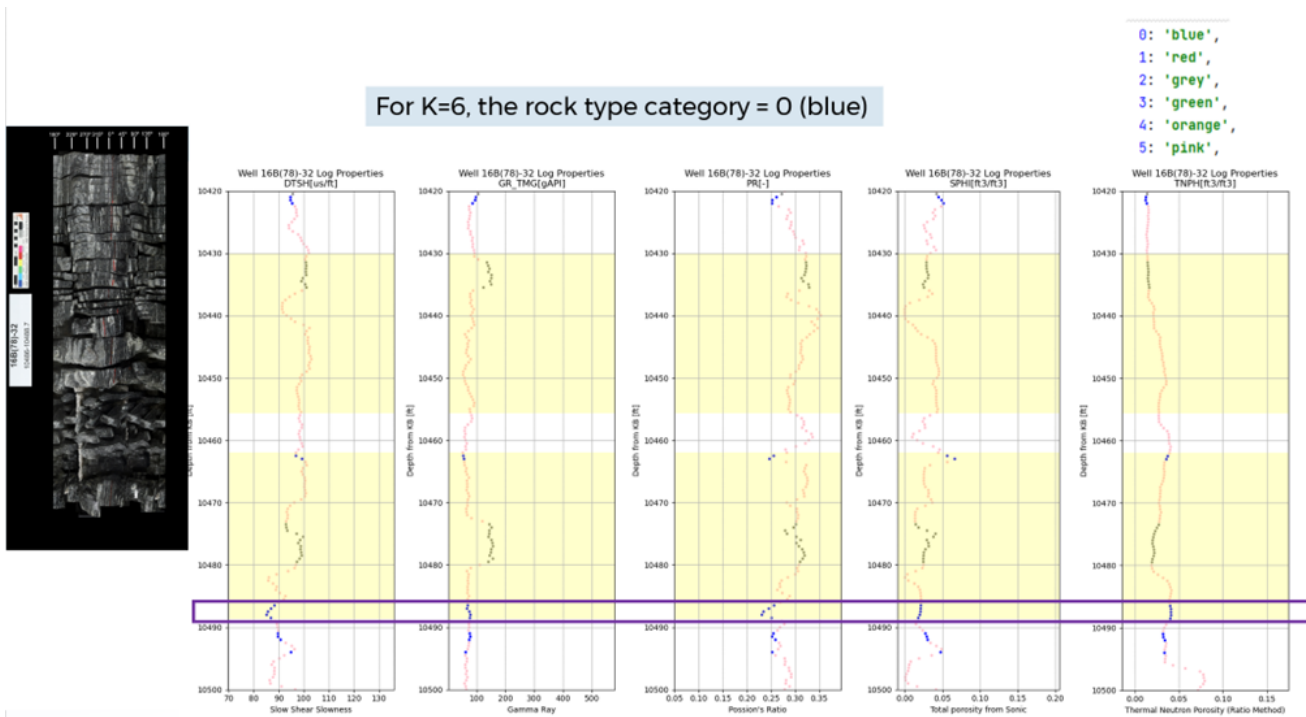

Figure 22. Comparing core from 16B(78)-32 at 10,486 ft KB to 10,488.7 ft KB to cluster label using k=6. Shaded yellow regions indicate where core is available.

2.4 Fracture Orientation

Fracture orientation data used to construct DFN models generally comes from wireline resistivity or acoustic logs that have been manually interpreted. The logs used in the current work are listed in Table 3.

Table 3. Interpreted resistivity log data sources used for fracture orientations and intensities.

Well	Log File	Fracture Categories used for DFN	Reference
58-32	University_of_Utah_MU_ESW1_FMI_HD_2226_7550ft_Dip_1stRun_Final.las	Conductive Continuous; Conductive Partially Resistive; Fault; Resistive Continuous	EGI, 2017
56-32	University of Utah FORGE 56-32 Monitor Well 3510_9070ft_TBFMI_Interpretation_Manual Dips.csv	Conductive Continuous; Conductive Non-Continuous; Conductive Lith Bound; Conductive Partially Resistive; Resistive Continuous	EGI, 2021a
16A(78)-32	University_of_Utah_Forge_16A-78-32_TBFMI_Interpretation_5040-10870ft_Cond_Cont_Frac_Outputs.las	Conductive Continuous	EGI, 2021b
78B-32	University_Utah_FORGE_78B-32_FMI_dips.las	Conductive Continuous; Conductive Non-Continuous; Conductive Partially Resistive; Resistive Continuous	EGI, 2021c
	University_Utah_FORGE_78B-32_UBI_dips.las	Low Acoustic Amplitude Continuous; Low Acoustic Amplitude Discontinuous	
16B(78)-32	Univ of Utah Forge 16B-78-32 TBFMI T3 TOH 6252-10914 DIPS.las	Conductive Continuous; Conductive Non-Continuous	EGI, 2023
	Univ of Utah Forge 16B-78-32 UBI T3 TOH 6252-8769 DIPS.las	Low Acoustic Amplitude Continuous; Low Acoustic Amplitude Non-Continuous	
	Univ of Utah Forge 16B-78-32 UBI T3 TOH 8769-9444 DIPS.las	Low Acoustic Amplitude Continuous; Low Acoustic Amplitude Non-Continuous	

Having established rock type boundaries in the well logs from the cluster analysis using six groups and confirming that the results are meaningful by comparison with core, the next step in determining if the DFN should treat these regions as distinct for fracture characterization is to examine fracture orientations in these intervals and see if they change in some systematic way.

2.4.1 Orientation in Highly Deviated Wells

Upper hemisphere stereonets of the fractures located in the rock type cluster intervals listed in Table 2 are shown for the lower, vertical portions of wells 16A(78)-32 and 16B(78)-32 in Figure 23. Well 16A(78)-32 has ThruBit Formation MicroImager (FMI) data while 16B(78)-32 has both ThruBit FMI and Ultrasonic Borehole Imager (UBI) data. All four previously identified sets seem to be present with the dominant set in the FMI data being the South-striking, moderately dipping West set while the UBI data seems to pick up the North-striking steeply dipping East set.

The two vertical sets striking SSW and East appear once the wells start to deviate from vertical (Figure 24). Once the wells start to deviate from vertical, the vertical SSW striking set is prominent in both 16A(78)-32 and 16B(78)-32 with some variability in strike. The South-striking, moderately dipping West set is present in the FMI data for 16A(78)-32 is both section 16A_K6_5 and 16A_K6_6, but is not visible in the 16B(78)-32 data.
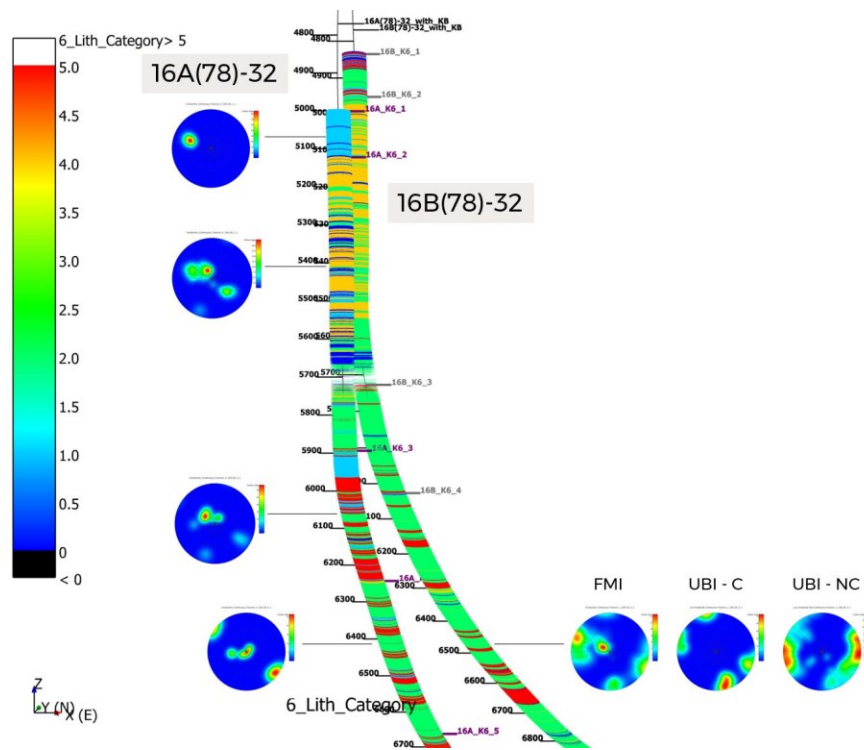
Figure 23. Fracture pole orientations plotted in upper hemisphere stereonets for vertical sections of wells 16A(78)-32 and 16B(78)-32. Wells are colored by cluster label number using k=6. Stereonets show FMI data unless otherwise labeled: "UBI-C" refers to Continuous fractures from the UBI log while "UBI-NC" refers to Non-Continuous fractures from the UBI log.
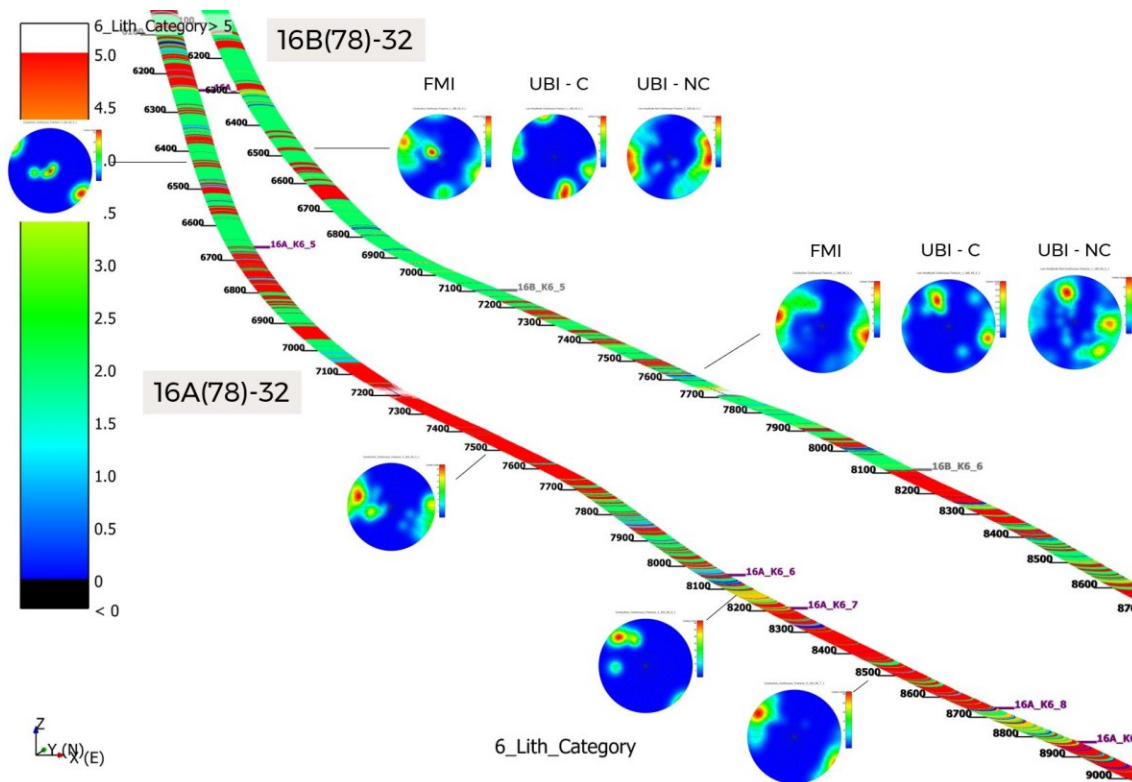

Figure 24. Fracture pole orientations plotted in upper hemisphere stereonets for the upper deviated sections of wells 16A(78)-32 and 16B(78)-32. Wells are colored by cluster label number using k=6.

17

In the middle part of the deviated sections, the vertical, SSW striking set is prominent in both wells with the vertical East-striking set present in the UBI data for 16B(78)-32, but not for the FMI data in either well (Figure 25). Finally, in the deepest sections of the wells, the vertical SSW striking set dominates with the South-striking moderately dipping West set appearing in 16A(78)-32 in the 16A_K6_12 interval(Figure 26).

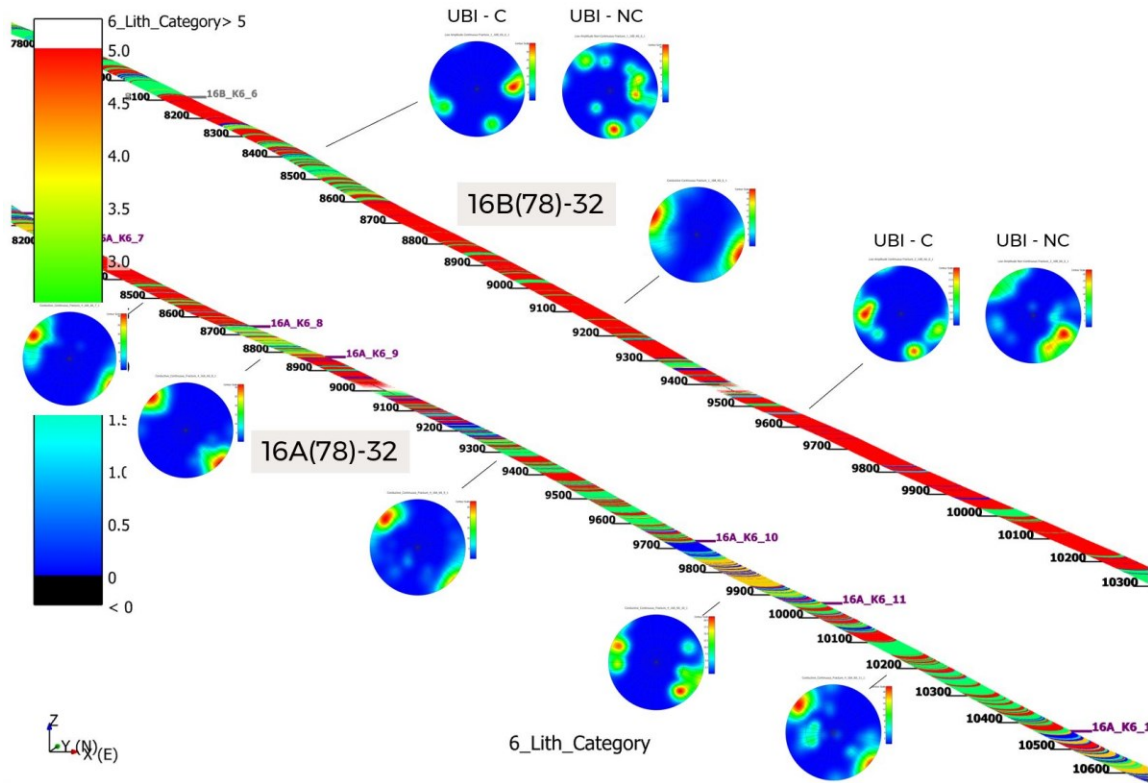**Figure 25. Fracture pole orientations plotted in upper hemisphere stereonets for the middle deviated sections of wells 16A(78)-32 and 16B(78)-32. Wells are colored by cluster label number using k=6.**
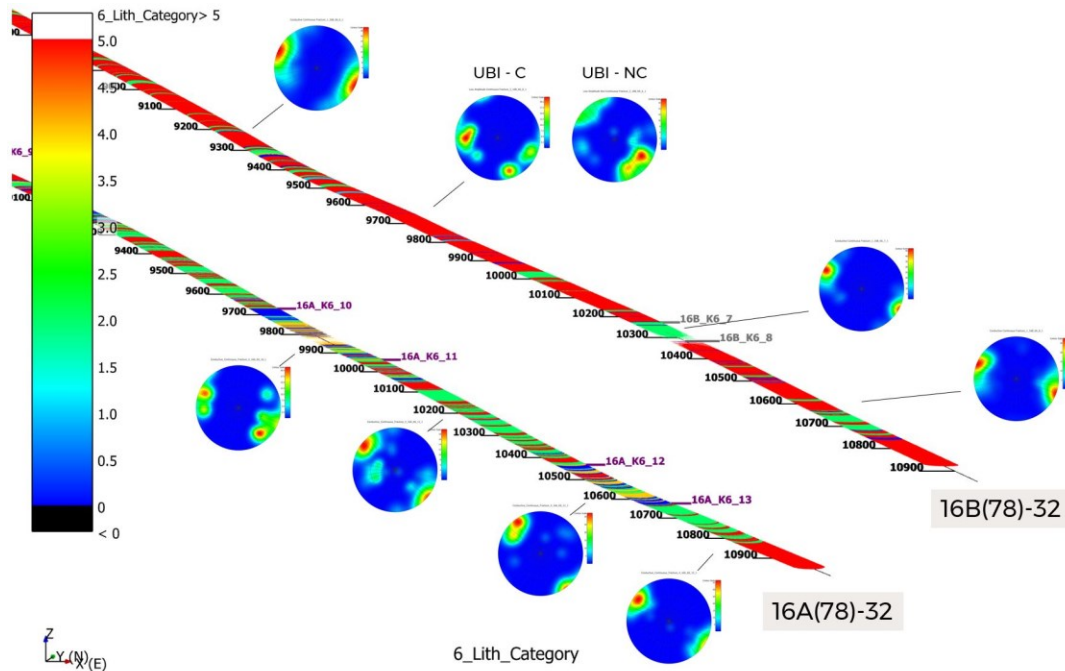

Figure 26. Fracture pole orientations plotted in upper hemisphere stereonets for the deepest deviated sections of wells 16A(78)-32 and 16B(78)-32. Wells are colored by cluster label number using k=6.

2.4.2 Orientation in Vertical Wells

In well 78B-32, there appear to be changes in fracture orientation between the rock cluster intervals (Figure 27). In the interval 78B_K6_1 (top blue section in Figure 27), there are several sets present including the vertical SSW-striking set and the South-striking, West dipping set. In intervals 78B_K6_2 and 78B_K6_3 (red sections in Figure 27), the vertical SSW-striking set is gone and the East-striking, steeply dipping South set appears. In well 56-32, the sets change between intervals 56-32_K6_3 and 56-32_K6_4, between 56-32_K6_ and 56-32_K6_5, between 56-32_K6_5 and 56-32_K6_6, and again between 56-32_K6_6 and 56-32_K6_7. Fracture orientations at the bottom of 56-32 are notably horizontal compared to other regions.
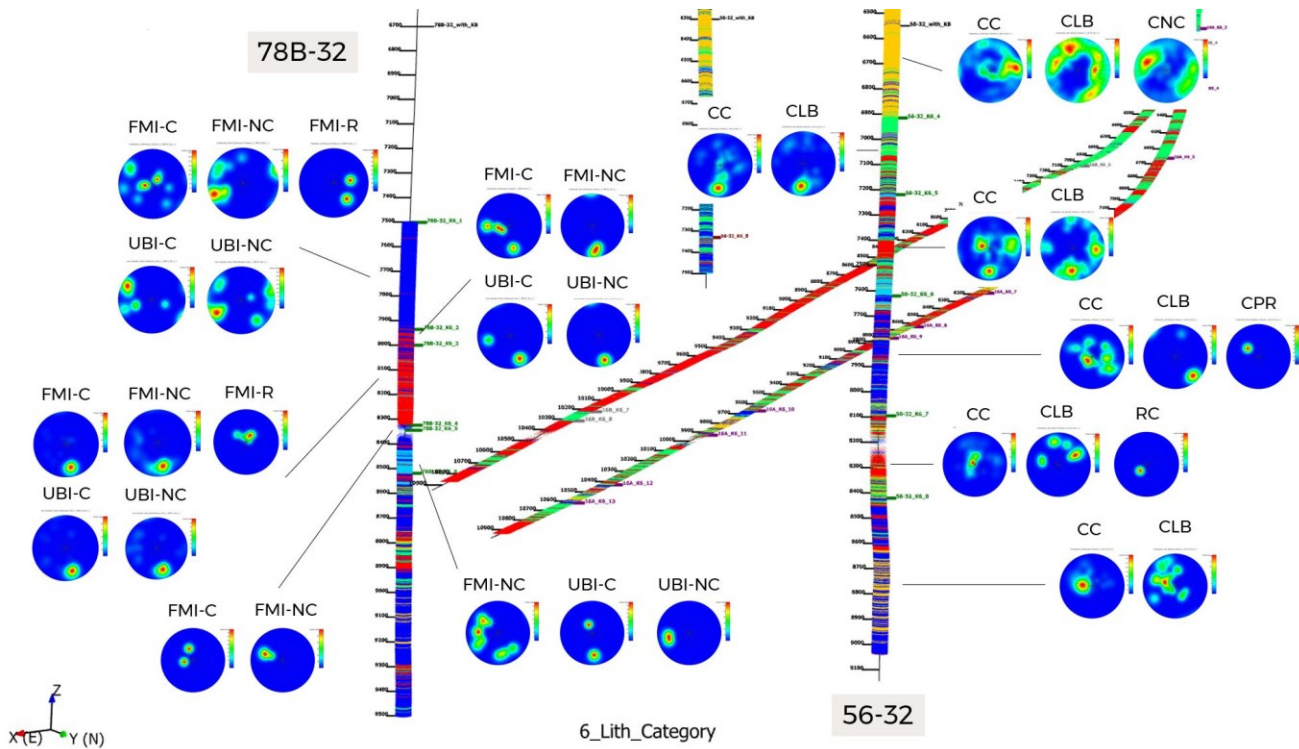

Figure 27. Fracture pole orientations plotted in upper hemisphere stereonets for vertical wells 78B-32 and 56-32. Wells are colored by cluster label number using k=6. Stereonets show different fracture categories as listed in Table 3.

Figure 28 repeats the stereonets for well 56-32 so then can be compared alongside of well 58-32. While both wells show the three sets identified in the 2019 DFN model, they do not include the vertical SSW-striking set apparent in the deviated wells and section 78B_K6_1 in well 78B-32. These two wells do show the East-striking, steeply dipping South set, so the difference does not appear to be caused by the well orientation bias.

From these figures, it looks like some of the interval divisions based on the rock cluster analysis do capture some changes in fracture orientation, although not all of them. Before combining any of the intervals where fracture orientations are the same, however, a similar exercise needs to be done with fracture intensity as shown in the following section.
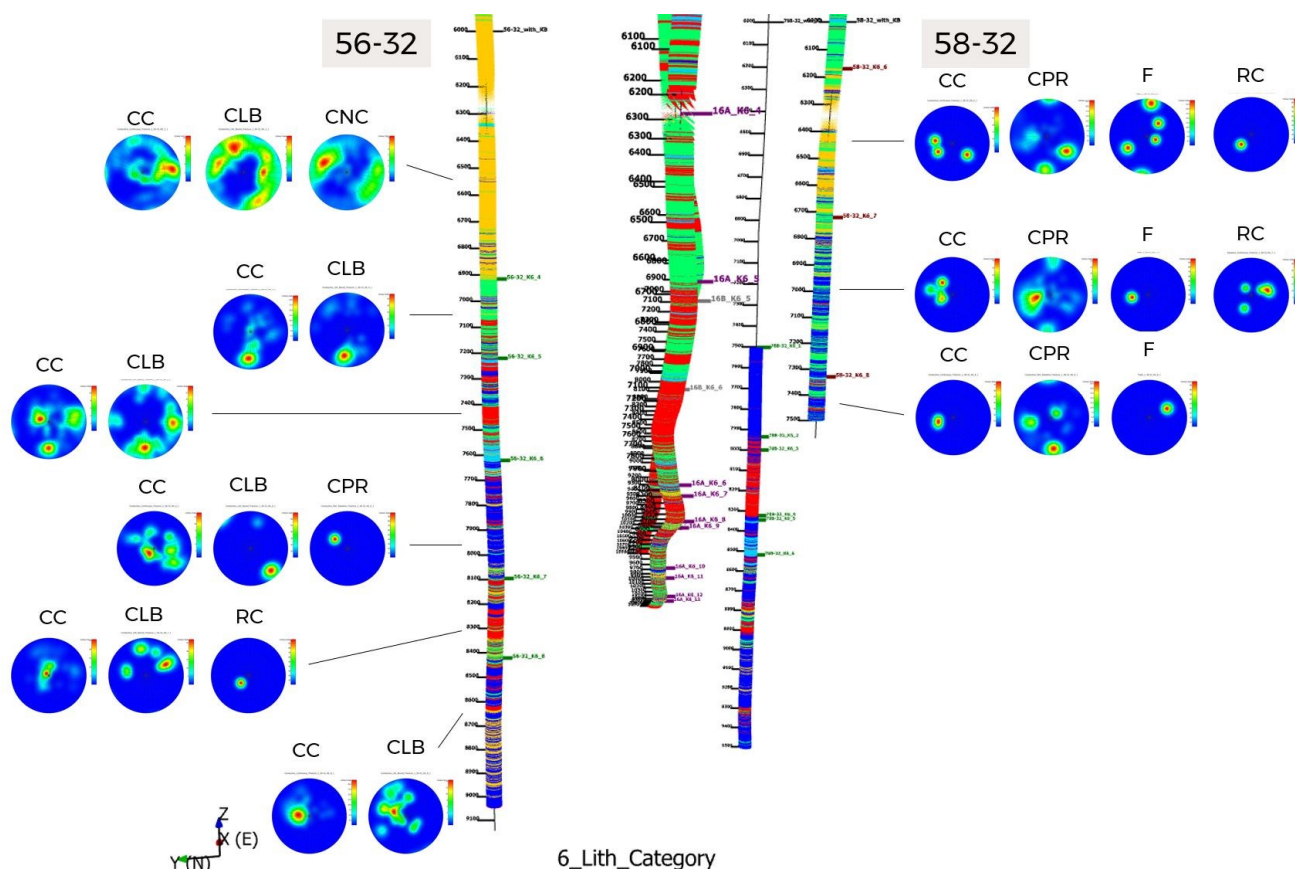
Figure 28. Fracture pole orientations plotted in upper hemisphere stereonets for vertical wells 56-32 and 58-32. Wells are colored by cluster label number using k=6. Stereonets show different fracture categories as listed in Table 3.

2.5 Fracture Intensity

The best source of fracture intensity in the FORGE reservoir region comes from the lineal fracture intensity, P_{10}, measured from the FMI or UBI log data. P_{10} is defined as the number of fractures per unit of length. This fracture intensity measurement is a function of both the well trajectory and the fracture set orientation, so needs to be converted to a P_{32} fracture intensity, fracture area divided by the volume. This fracture intensity measurement is independent of the well trajectory or fracture orientations and even sizes, so it is a better measure to use when comparing relative fracture intensities. To convert between the P_{10} and P_{32} values, a Terzaghi weight (Terzaghi, 1965) was calculated using a maximum value of 7 and the P_{32} values were then calculated as the sums of the Terzaghi weights in the interval divided by the interval length. Table 4 shows the fracture intensity values for each rock type cluster interval which lie within the DFN model region. The presence of the orientation sets is also indicated so that adjacent intervals can be compared using both fracture orientation and intensity. The intent was to find similar contiguous intervals which could then be combined to simplify the subdivisions.

Table 4. Fracture set presence and fracture intensity measures P_{10} and P_{32} for the rock cluster intervals identified using k=6. Sets are labeled using the strike direction followed by the dip direction if not vertical. Letter for yes (Y/y) and no (N/n) indicate if the set is present and the use of capital letters implies more certainty. Intervals missing entries either lie outside the DFN model region or do not have complete data sets.

Well	Interval Name	Strike S Dip W	Strike E Dip S	Strike N Dip E	Strike SSW	FMI P_{10} [1/ft]	FMI P_{32} [1/ft]
16A(78)-32	16A_K6_1	Y	N	N	N	0.108	0.158
	16A_K6_2	Y	y	y	N	0.041	0.065
	16A_K6_3	Y	y	y	n	0.052	0.090
	16A_K6_4	y	N	N	Y	0.014	0.029
	16A_K6_5	Y	N	n	Y	0.029	0.041

	16A_K6_6	y	N	N	Y	0.040	0.048
	16A_K6_7	N	N	N	Y	0.137	0.170
	16A_K6_8	N	N	N	Y	0.183	0.284
	16A_K6_9	n	N	N	Y	0.103	0.161
	16A_K6_10	n	N	Y	Y	0.049	0.068
	16A_K6_11	Y	y	y	Y	0.119	0.170
	16A_K6_12	N	N	y	Y	0.179	0.254
	16A_K6_13	N	N	N	Y	0.187	0.273
16B(78)-32	16B_K6_1						
	16B_K6_2						
	16B_K6_3						
	16B_K6_4	Y	Y	N	Y	0.237	0.309
	16B_K6_5	y	y	n	Y	0.395	0.535
	16B_K6_6	Y	Y	Y	Y	0.377	0.511
	16B_K6_7	y	N	N	Y	0.335	0.395
	16B_K6_8	N	N	N	Y	0.487	0.633
56-32	56-32_K6_1					0.740	0.977
	56-32_K6_2					0.434	0.929
	56-32_K6_3	y	y	Y	Y	0.218	0.733
	56-32_K6_4	N	Y	y	y	0.434	1.125
	56-32_K6_5	Y	Y	Y	N	0.414	1.073
	56-32_K6_6	Y	N	Y	Y	0.112	0.232
	56-32_K6_7	Y	N	Y	y	0.331	0.493
	56-32_K6_8	Y	N	n	Y	0.224	0.343
58-32	58-32_K6_1					0.111	0.187
	58-32_K6_2					0.739	1.313
	58-32_K6_3					0.334	0.703
	58-32_K6_4					0.362	0.756
	58-32_K6_5					0.434	1.150
	58-32_K6_6	Y	Y	Y	N	0.335	1.016
	58-32_K6_7	Y	Y	Y	N	0.263	0.609
	58-32_K6_8	Y	Y	Y	N	0.623	1.766
78B-32	78B-32_K6_1	Y	N	y	Y	0.046	0.095
	78B-32_K6_2	Y	Y	N	N	0.062	0.128

	78B-32_K6_3	N	Y	N	N	0.222	0.627
	78B-32_K6_4	Y	N	N	N	0.098	0.122
	78B-32_K6_5	Y	Y	N	y	0.000	0.000
	78B-32_K6_6						

The fracture intensity in individual intervals may also be evaluated using a Cumulative Fracture Intensity Plot (CFI) where the slope of the line shows the inverse of the P_{10} value; so higher slopes correspond to lower fracture intensities. Figure 29 shows interval 16A_K6_5 of well 16A(78)-32 which is color coded to show the clustering using six groups. The fracture intensity is very heterogeneous along the length of this interval with very few fractures at depths below approximately 7750 ft.
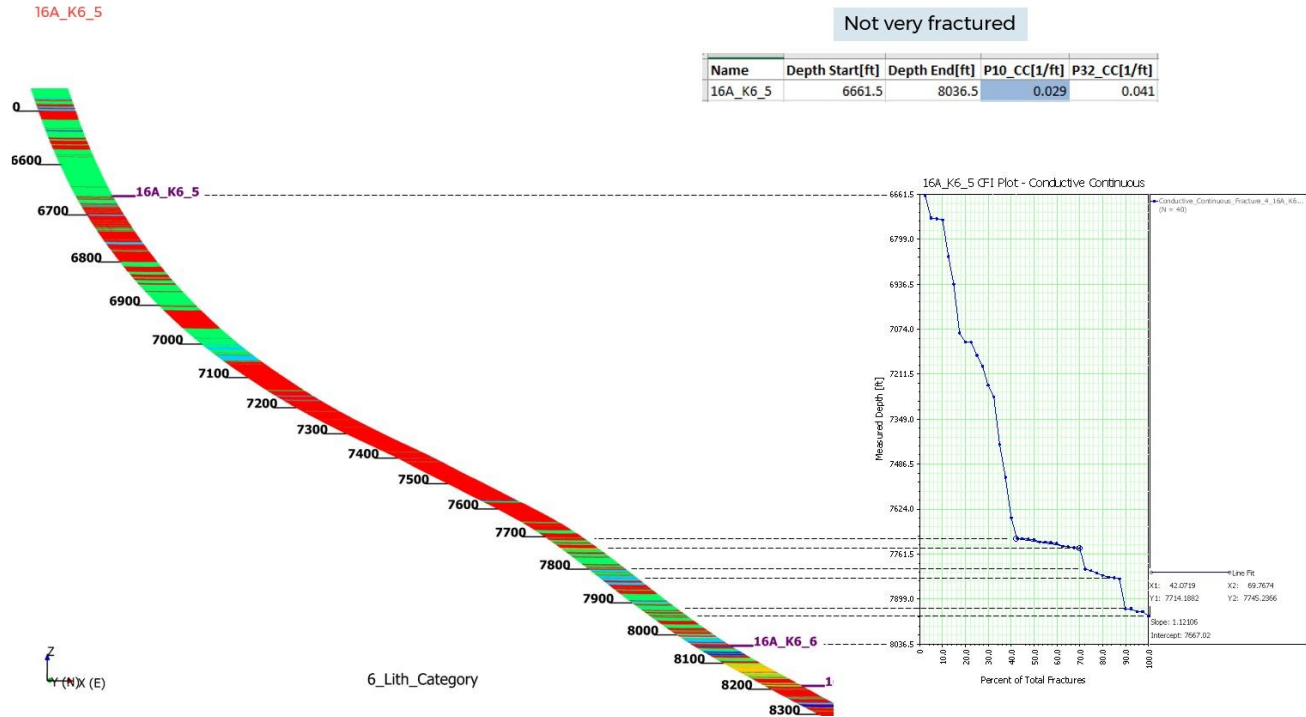

Figure 29. CFI plot next to a section of well 16A(78)-32 which is color coded to show the clustering using k=6.

One other consideration for determining the DFN fracture intensity is to try and estimate any bias in the FMI or UBI interpretation. Would we generally expect to over or underestimate fractures based on these log interpretations? Fortunately, we have overlapping core and interpreted logs in well 16B(78)-32 where we can check this. An example is shown in Figure 30 where a three-foot core length is compared in photo (unwrapped to show full circumference) with the pdf file of the image log. In this instance, it looks like the interpreter may have missed a couple of fractures as none were identified in the FMI image while two planar features present in the core look like natural fractures. It can be hard to tell if a fracture in the core is a natural fracture or a mechanical break, especially if just using a photo, however, the high quality of both the photographs and the image logs make this a meaningful check.
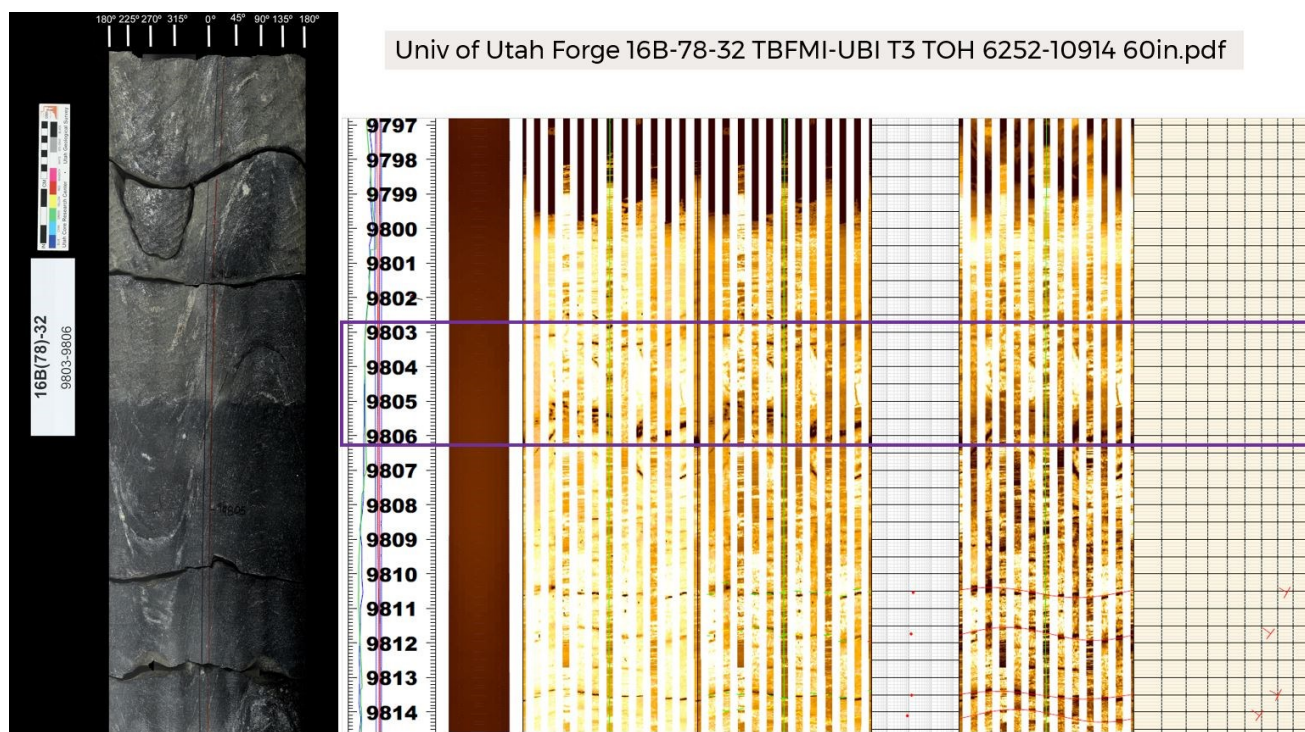
Figure 30. Comparison between core from well 16B(78)-32 and the FMI interpretation.

3. IDENTIFYING SIGNIFICANT FAULTS OR FRACTURE ZONES

As mentioned in the cluster analysis discussion for the case of k=2, where the acoustic log data was divided into two groups, the division found the alluvium in the shallow depths of well 58-32 as well as some small zones in deeper sections of four of the five deep wells. Table 5 shows these zones which have lengths ranging from half a foot to 8.5 ft. These locations are shown in Figure 31 without attempting to orient any possible planar feature that may be causing the interval to display acoustic properties closer to alluvium than bedrock.

Table 5. Significant fracture zones based on a cluster analysis with k=2.

Well	Depth Start KB [ft]	Depth End KB [ft]	Length [ft]	Mid-Point [ft]
16A(78)-32	5064.5	5069.0	4.5	5066.75
	6147.5	6148.5	1.0	6148.00
	7828.5	7829.5	1.0	7829.00
	7895.5	7897.0	1.5	7896.25
	8013.0	8015.0	2.0	8014.00
	8252.5	8254.0	1.5	8253.25
	10039.0	10041.0	2.0	10040.00
16B(78)-32	4951.0	4953.5	2.5	4952.25
	5089.0	5091.0	2.0	5090.00
	7580.5	7581.0	0.5	7580.75
	7583.5	7587.5	4.0	7585.50
56-32	6340.0	6341.5	1.5	6340.75

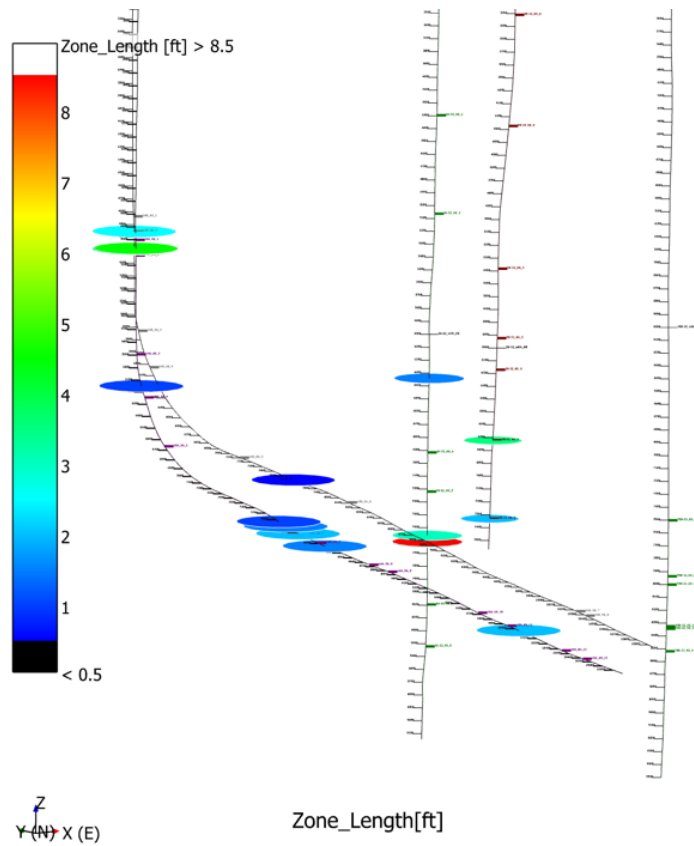|	7558.5	7561.5	3.0	7560.00
	7604.5	7613.0	8.5	7608.75
	7615.0	7618.0	3.0	7616.50
58-32	6720.0	6723.5	3.5	6721.75
	7329.5	7331.5	2.0	7330.50

Figure 31. Potential faults or major fracture zones as identified in cluster analysis with k=2. Orientation of these features in generally unknown but the discs are color coded to indicate the length of the zone.

We are fortunate to have an orientation for one of these features in well 58-32. There were several faults identified from the FMI log in well 58-32 and one of them corresponds with the zone found using the cluster analysis (Figure 32). This fault shares the general orientation of the west-dipping bedrock surface and aligns with the South-striking, west-dipping fracture set. If the FMI or UBI logs can suggest orientations for these features, then they can be added as discrete features to the DFN. Once oriented, extending them to see where they intersect with other wells also may yield bounding surfaces for subdividing the DFN region into fault blocks.
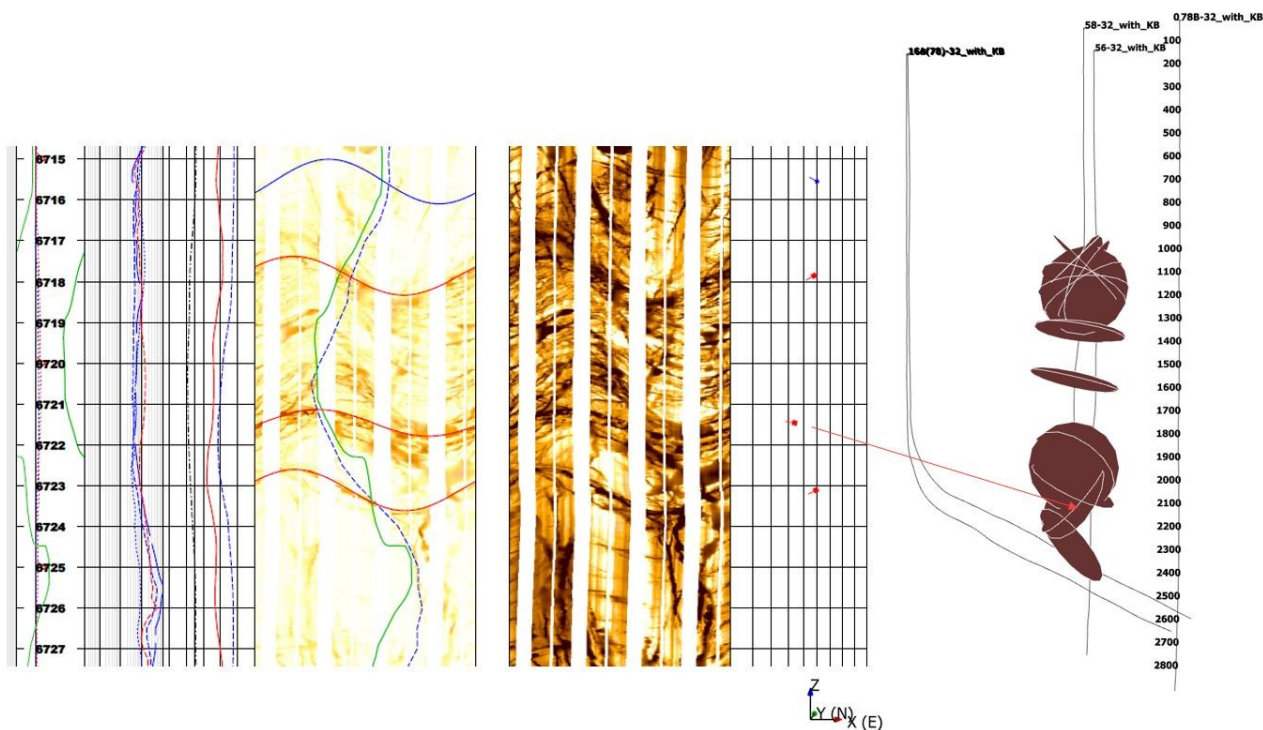
Figure 32. Fault identified from resistivity log in well 58-32.

4. SELECTING FRACTURES FOR THE DISCRETE FRACTURE SETS

Previous versions of the Reference DFN model included discrete fracture sets for fractures intersecting the wellbore in the model region. This was done by 1) first generating the stochastic fractures to fill the model region; 2) removing all stochastic fractures that intersected the wellbore where fracture logs were available; and 3) adding in all or a subset of the fractures identified in the fracture log. While these fracture locations and orientations were known, their sizes were generally unconstrained so if we only wanted the largest 5% of these features, we would generally just randomly select them from the intersecting set. By utilizing other log data in this process, such as the acoustic data we used in the cluster analysis, we can now selectively choose identified fractures that lie closest to any spikes in these logs, such as the one of the porosity logs shown in Figure 15 and Figure 16. A threshold value can be chosen to select the appropriate number of fractures that are desired for the DFN.

5. BUILDING THE REVISED DFN

In this section we put all the prior analyses and observations together to build the updated Reference DFN model.

5.1 Model Region

The model region is larger than in the previous Reference DFN models with dimensions of 1800 m x 1500 m x 1000 m (5905 ft x 4921 ft x 3281 ft) and located approximately between depths of 6500 ft to 9800 ft below the surface (Figure 33). The model region is rotated 20° from the N-S and E-W global coordinate frame so that the local coordinate frame is aligned with the principal horizontal stress directions with SHmax (σ2) at N20°E and Shmin (σ3) at N110°E. This allows for easier interpretation of tensor values calculated using a local coordinate frame that is aligned with the principal stresses.
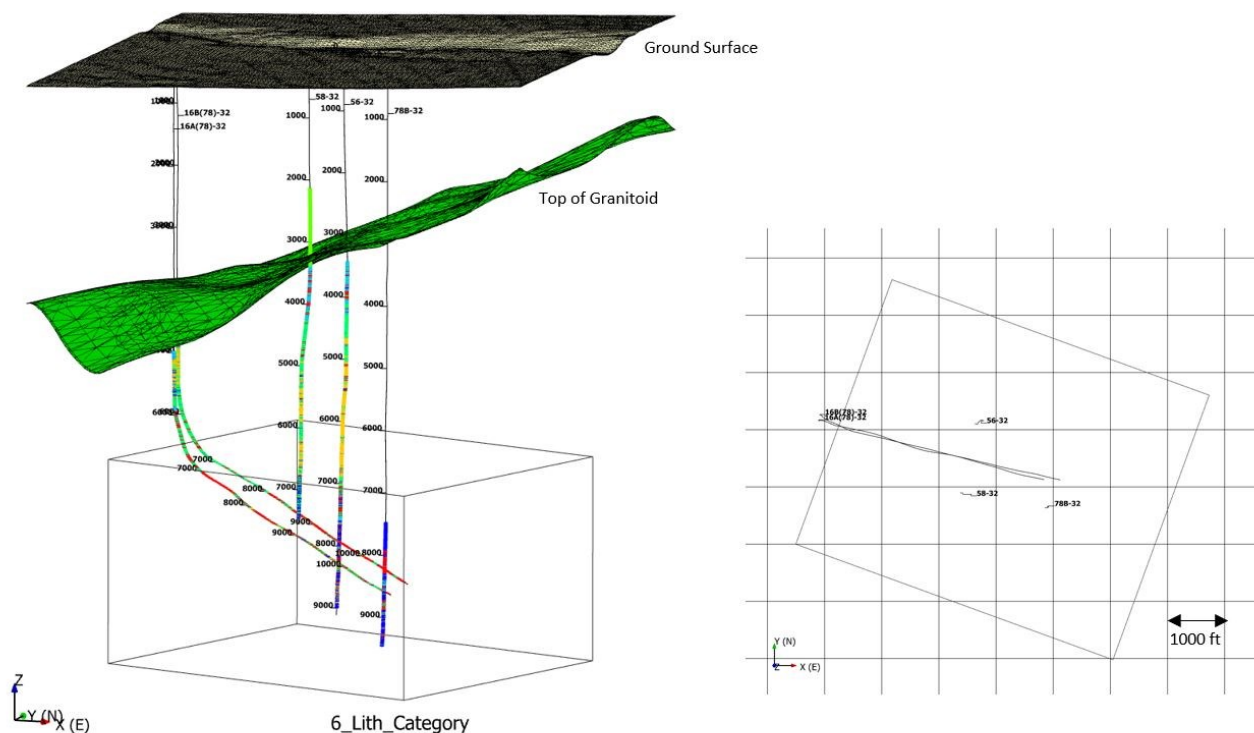
Figure 33. Side and top-down views of the DFN model region. Wells are colored using the cluster results for k=6.

5.2 Dividing the Model Region into Different Subregions

While there is an ongoing effort to delineate the distinct subregions in the model, currently the geometry appears to be too complex to incorporate. While correlations can be made between the vertical wells, the deviated wells which pass between wells 58-32 and 56-32 seem to have distinct patterns of fracture orientation and intensity. Additionally, it is not clear yet whether to include the deviated wells in the same subregion or divide them. We have made progress on finding discrete faults or fracture zones which can be added to the model now and may be used in the future to define distinct fault blocks.

5.3 Stochastic Fracture Set

5.3.1 Fracture Orientation

Fracture orientations identified in each well that fall in the new model region are shown in Figure 34. The same four orientation sets are present as had been previously identified in the 2021 Reference DFN model, although mean orientation poles and Fisher concentrations parameters have been adjusted to incorporate the additional data from the two newer wells. Table 6 lists the updated values for the set mean pole orientation, the Fisher concentration parameter, and the relative intensities.

It is notable that the orientation patters are so different in the deviated wells compared with the vertical wells. In the deviated wells, the vertical, SSW striking set dominates. With the vertical wells, the East striking, steeply dipping south set dominates. The south striking, moderately dipping west set is present in wells 56-32 and 58-32, but not a major set in well 78B-32. The north striking steeply dipping east set is only significant in well 56-32 but may be represented in 78B-32 with the strike rotated a bit to the North and the dip less steep. Fracture intensity in well 16B(78)-32 appears to be approximately 4 times that in well 16A(78)-32 based on point density in the stereonets (370 fractures in 16A(78)-32 and 1594 fractures in 16B(78)-32).
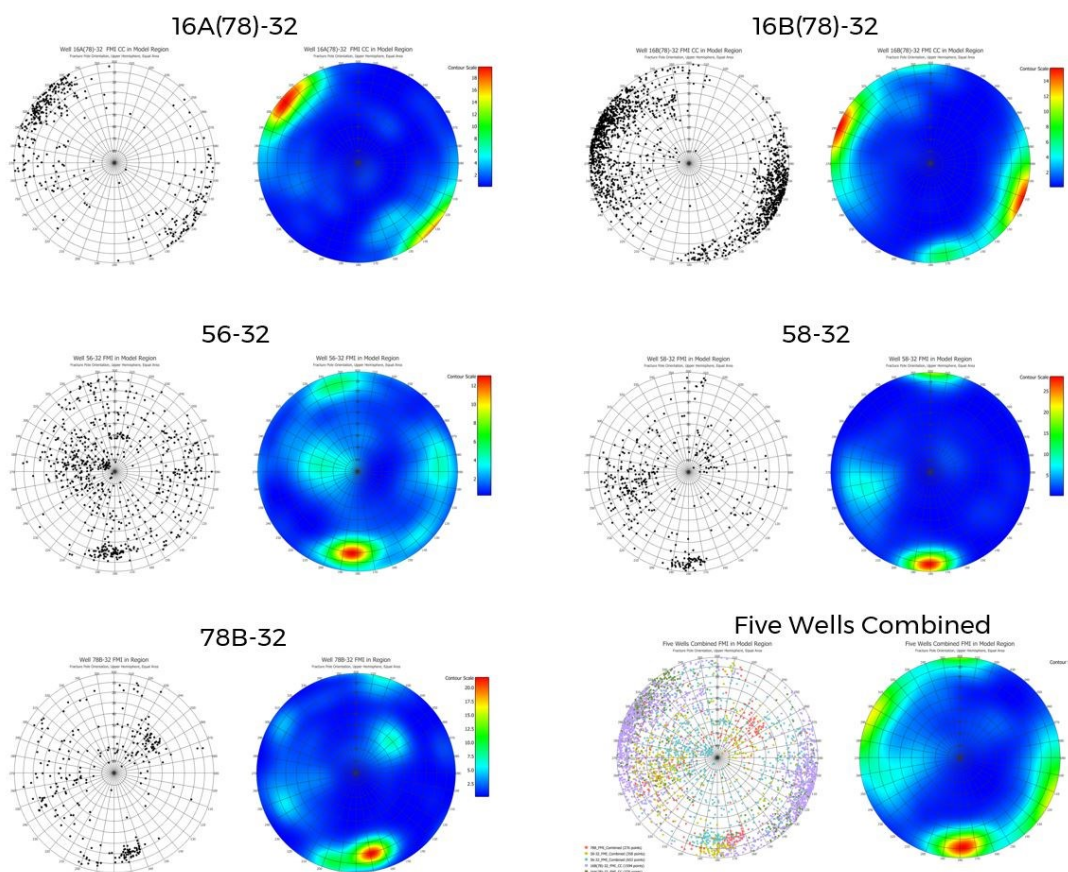
Figure 34. Upper hemisphere, equal area stereonets of FMI fractures in DFN model region. Contour plots include Terzaghi weighting.

Table 6. Updated fracture set parameterization.

Set Name	Description	Trend/Plunge [deg]	Strike/Dip [deg]	Fisher Concentration	%
Set 1	East-striking, sub-vertical dipping South	358/12	88/78	20	35
Set 2	SSW-striking, vertical	115/3	205/87	15	35
Set 3	South-striking moderately dipping West	75/35	165/55	10	20
Set 4	North-striking, moderately dipping East	230/50	320/40	7	10

5.3.2 Fracture Size and Shape

No changes were made to the parameterized fracture size distribution or choice of fracture shape in the current revision. The model still uses a truncated power law distribution having a power law exponent of 3.2 and a minimum fracture radius of 0.63 m. The DFN uses a larger minimum size cutoff of 20 m for the equivalent radius (R_e) of the fracture (compared to the previous 10 m size in the 2021 Reference DFN), and the same maximum size cutoff of 150 m as the previous model. The R_e of a fracture is defined as the radius of a circle having the same fracture area as the actual fracture (which may not be circular). Fractures are still assumed to have roughly circular shapes and are included as planar hexagons.

5.3.3 Fracture Intensity

Fracture intensity has been averaged over the model region using the P_{10} and P_{32} data from each of the five wells (Table 7). The DFN uses the interval length weighted P_{32} fracture intensity of 0.417 1/ft (1.367 1/m). This is higher than that used in the 2021 Reference DFN model which used a P_{32} value of 1.15 1/m. The higher value is due to the higher fracture intensity in well 16B(78)-32 and the change in modeling region. When generating the stochastic fracture sets in the reference DFN for fractures having an equivalent radius between 20 m and 150 m, the P_{32} values are adjusted by a factor of 0.0143 for a total P_{32} in the stochastic sets of 0.0196 1/m.

Table 7. Fracture intensity inside the DFN model region.

Well	Interval Length [ft]	P_{10} [1/ft]	P_{32} [1/ft]	P_{10} [1/m]	P_{32} [1/m]	Truncated P_{32} [1/m] for 20 m < R_e < 150 m
16A(78)-32	3985	0.093	0.130	0.304	0.427	
16B(78)-32	4299	0.371	0.511	1.217	1.677	
56-32	2615	0.251	0.553	0.824	1.814	
58-32	994	0.356	0.952	1.168	3.125	
78B-32	1893	0.146	0.336	0.478	1.101	
Well Average		0.243	0.496	0.798	1.629	
Interval Length Weighted Average		0.236	0.417	0.773	1.367	0.0196

5.4 Discrete Features

After generating the stochastic fracture sets, all stochastic fractures intersecting the wells are removed and a discrete fracture set is added for each well. An additional eleven fractures are added from the 2023 DFN which were interpreted as planar features in the microseismic point data cloud from the simulation of well 16A(78)-32 (Finnila et al., 2023). For the well discrete fracture sets, the significant faults or fracture zones identified during the clustering process and listed in Table 5 are individually examined and compared with FMI image logs provided in pdf format to attempt to determine orientations. If no nearby fracture or fault has been identified in the image log, the orientation is set to be the same as one of the intersecting stochastic fractures removed from the model. Additional fractures are added based on either estimated apertures (if available) or porosity logs to match the approximate number and size of the stochastic fractures that were removed. All discrete fractures are shown in Figure 35.
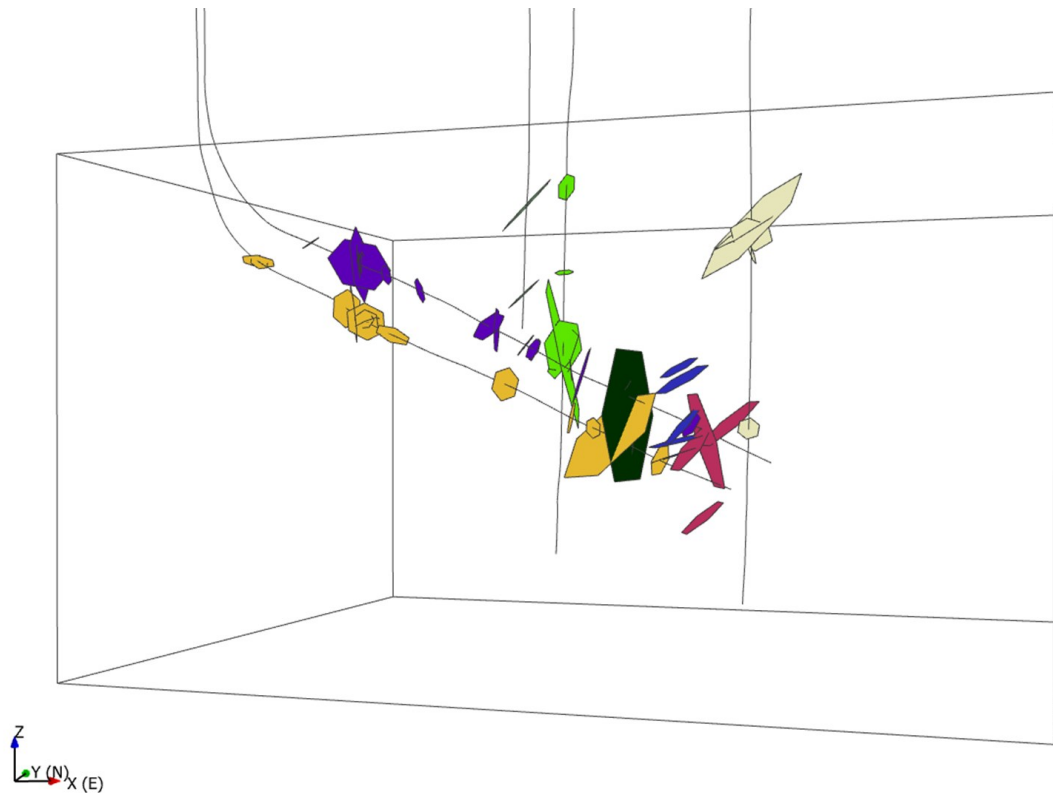

Figure 35. Discrete fracture sets included in the Reference DFN.

6. DISCUSSION

The additional data provided by two deep wells at the FORGE site have highlighted the complexity of the natural fracture orientations and intensity. The updated Reference DFN includes adjusted fracture set orientations and intensities and many new discrete features representing significant faults or fracture zones.

We briefly discuss the questions that were included in the Introduction.

6.1 Do we have sufficient data now to subdivide the Reference DFN into different regions having distinct fracture set populations based on fracture orientations or intensity?

After a significant level of effort, this is still not feasible. The rock type cluster analysis included in this paper seemed to be successful at identifying sections of each logged well having similar responses to the downhole acoustic tool as was minimally verified using core samples for comparison. The issue seems to be that the bedrock compositions and mechanical properties are quite heterogeneous and change over relatively small distances, so breaking the reservoir down into two or three subregions seems difficult. It is difficult correlating between the wells, even between well 16A(78)-32 and 16B(78)-32 which are within 330 ft (100 m) of each other and have similar trajectories. It remains puzzling that the fracture orientations as interpreted from the deviated wells are distinct from the surrounding vertical wells.

6.2 Can we identify any significant faults or fracture zones that can be added to the DFN as discrete features?

Yes, there has been excellent progress with this effort and several features have now been identified in each well bore which are now included in the Reference DFN. Combining the fracture interpretations from the resistivity logs with the cluster analysis performed on the acoustic logs is proving to be a valuable process.

6.3 Can we provide a rationale for selecting which identified fractures from the well logs to include in the discrete fracture set?

We are now using the rock type cluster results to identify some of the most significant, high-porosity features that have been located from the resistivity logs, which solves part of this issue. Further work with some underutilized fracture aperture estimates available from the fracture identification process also allow a ranking to be made of the identified fractures, so that those having the largest measured apertures values can be included in the DFN.

6.4 Can we explain why the interpreted fracture orientations and intensities were so different in well 16A(78)-32 vs the two vertical wells 58-32 and 56-32 used in the 2021 DFN?

This is still hard to explain. With the presence of nearby faults such as the Mag Lee Fault and the Opal Mound Fault along with numerous smaller faults, it seems possible that the reservoir could be compartmentalized into distinct fault blocks, however, that is just one hypothesis and there may be other explanations.

6.5 Does the DFN show connectivity that is consistent with well testing data?

The point of this question is to address the seeming contradictory observations that the fracture model is generally well connected given the estimated fracture intensity, orientations, and size distribution, however the *in situ* (pre-stimulation) permeability is negligible and the reservoir generally behaves as a closed system. This could indicate that fracture intensities should be lower in the DFN model, but there may be other explanations such as having strong infilling of fractures or unrecognized sealing boundaries.

7. CONCLUSION

The FORGE Reference DFN has been updated to reflect the additional data collected and analyzed since the last major revision in 2021. A clustering algorithm was used on acoustic log data for each of the current five deep wells in order to identify changing rock types or mechanical properties. This exercise provided rationale for including several new discrete features into the DFN model. The rock type classification along the well bores shows the significant heterogeneity of the reservoir rock where plutonic granitoids intermingle with metamorphic rock. Simple boundaries between major rock types were not established, instead, the evidence points to sheared zones or mixed melting at lithologic boundaries. While the four fracture sets identified in the 2021 revision remain, the overall fracture intensity in the DFN has increased and the relative proportions of each set in the new, larger model region have been adjusted.

Finnila and Jones

REFERENCES

Energy and Geoscience Institute at the University of Utah. (2017). Utah FORGE: Well 58-32 Schlumberger FMI Logs DLIS and XML files [data set]. Retrieved from https://dx.doi.org/10.15121/1464529.

Energy and Geoscience Institute at the University of Utah. (2018). Utah FORGE: Logs and Data from Deep Well 58-32 (MU-ESW1) [data set]. Retrieved from https://dx.doi.org/10.15121/1452735.

Energy and Geoscience Institute at the University of Utah. (2021a). Utah FORGE: Well 56-32 Drilling Data and Logs [data set]. Retrieved from https://dx.doi.org/10.15121/1777170.

Energy and Geoscience Institute at the University of Utah. (2021b). Utah FORGE: Well 16A(78)-32 Logs [data set]. Retrieved from https://dx.doi.org/10.15121/1777912.

Energy and Geoscience Institute at the University of Utah. (2021c). Utah FORGE Well 78B-32 Daily Drilling Reports and Logs [data set]. Retrieved from https://dx.doi.org/10.15121/1814488.

Energy and Geoscience Institute at the University of Utah. (2023). Utah FORGE: Well 16B(78)-32 Logs from Schlumberger Technologies [data set]. Retrieved from https://dx.doi.org/10.15121/2001059.

Finnila, A., Forbes, B., and Podgorney, R.: Building and Utilizing a Discrete Fracture Network Model of the FORGE Utah Site, Proceedings, 44th Workshop on Geothermal Reservoir Engineering, Stanford University, Stanford, CA (2019).

Finnila, A.: Estimation of Fracture Size for a Discrete Fracture Network Model of the Utah FORGE Geothermal Reservoir using Forward Modeling of Fracture-Borehole Intersections, paper presented at the 55th U.S. Rock Mechanics/Geomechanics Symposium, physical event cancelled, originally accepted for the 3rd International Discrete Fracture Network Engineering Conference. DFNE 21-2329 (2021).

Finnila, A., Doe, T., Podgorney, R., Damjanac, B., and Xing, P.: Revisions to the Discrete Fracture Network Model at Utah FORGE Site, GRC Transactions, Vol. 45, (2021).

Finnila, A. and Jones, C.: Rapid Rock Type Categorization at Utah FORGE from Sonic Logs using K-Means Clustering, GRC Transactions, Vol. 46, (2022).

Finnila, A., Damjanac, B. and Podgorney, R.: Development of a Discrete Fracture Network Model for Utah FORGE using Microseismic Data Collected During Stimulation of Well 16A(78)-32, Proceedings, 48th Workshop on Geothermal Reservoir Engineering, Stanford University, Stanford, CA, (2023), SGP-TR-224.

Fu, W., Damjanac, B., Radakovic-Guzina, Z., Finnila, A., Podgorney, R., and McLennan, J.: Near-Wellbore DEM Model of Hydraulic Fracture Initiation for Utah FORGE Site, Proceedings, 49th Workshop on Geothermal Reservoir Engineering, Stanford University, Stanford, CA (2024).

Jones, C. G., Moore, J. N., and Simmons, S. F.: X-ray diffraction and Petrographic Study of Cuttings from Utah FORGE Well 16A(78)-32, GRC Transactions, 45, (2021).

Radakovic-Guzina, Z., Damjanac, B., Fu, W., Finnila, A., Podgorney, R., and McLennan, J.: Coupled Hydro-Mechanical Back-Analysis of Circulation Program at FORGE in July of 2023, Proceedings, 49th Workshop on Geothermal Reservoir Engineering, Stanford University, Stanford, CA (2024).

Terzaghi, R.: Sources of Error in Joint Surveys, Géotechnique, 15, (1965), 287-304.

WSP UK: FracMan® Reservoir Edition, version 8.2 Discrete Fracture Network Simulator, (2023).